Optical Contrast between Transparent Materials through External Modulation of the Faraday Effect

by

Timothy Allman Denison

Submitted to the Department of Electrical Engineering and Computer Science
in partial fulfillment of the requirements for the degree of

Master of Science in Electrical Engineering

at the

MASSACHUSETTS INSTITUTE OF TECHNOLOGY

January 1998

Author .....
Department of Electrical Engineering and Computer Science
January 18, 1998

Certified by .....
Steven B. Leeb
Carl Richard Soderberg Assosciate Professor of Electrical Engineering
Thesis Supervisor

Accepted by .....
Arthur C. Smith
Chairman, Department Committee on Graduate Students

Optical Contrast between Transparent Materials through External Modulation of the Faraday Effect

by

Timothy Allman Denison

Submitted to the Department of Electrical Engineering and Computer Science
on January 18, 1998, in partial fulfillment of the
requirements for the degree of
Master of Science in Electrical Engineering

Abstract

This thesis successfully demonstrates the use of the Faraday effect as a contrast mechanism for transparent materials. Existing contrast techniques generally rely on measurements of optical properties at low frquencies or DC. Low frequency measurements limit the ability to resolve small variations in materials due to drift noise in the detection system. The use of external modulation of a material's optical properties allow them to be shifted outside of the region of large 1/F noise. The application of synchronous detection to the modulated optical signal then allows for increased resolution of small material variations. Several methods of optical modulation are discussed, including stress, electric and magnetic fields. Of these, it is found that the Faraday effect is the most practical to implement.

The advantages of the Faraday effect for external modulation include the rapid penetration of an external magnetic field into a sample and the large range of Verdet constants. These principles are employed in a polarization sensitive instrument that externally modulates a magnetic field. The transmitted light intensity is then synchronously detected with respect to the varying magentic field. This instrument established contrast in transparent materials that could not be differentiated by amplitude modulation properties alone. Future applications of this contrast approach include the imaging of translucent tissues and structures with deeply penetrating wavelengths.

Thesis Supervisor: Steven B. Leeb
Title: Carl Richard Soderberg Assosciate Professor of Electrical Engineering

Acknowledgments

I would like to thank Steve Leeb for letting me pursue this topic which has fascinated me since I was an undergraduate Physics student. His support was crucial to the success of the project. In addition, my OQE committee, Profesors Roberge, Fonstad, and Sodini, helped to clarify some of the issues in this thesis.

My family, Mom, Pop and Heather, deserve a lot of credit for fostering my interest in engineering. I appreciate the help my parents gave to old science fair projects, and tolerating so much questionable behavior with a sense of humor and more patience than I deserved.

I would also like to express my appreciation to several members of the MIT community who helped in the construction of the imaging instrument. Terry Herndon, an all-around great engineer supplied the Glan-Thomson polarizers and general encouragement. The Physics lecture demos group have patiently loaned me their electromagnets, pulleys, and such for a year now. Professor Warde has generously supplied me with materials and lab space in his Modern Optics lab. Finally, Professor Ram has provided many interesting pointers throughout the project.

That leaves my wife Kristen. Covering her help would be another thesis, longer and much more interesting. Its a kinda magic...

Contents

List of Figures

List of Tables

Chapter 1

Introduction

1.1 Background and Motivation

The imaging of transparent or translucent objects has led to several interesting contrast mechanisms in microscopy and tomography. Staining and fixing techniques were developed in the nineteenth century to resolve structural properties of transparent biological objects. Barium and other external contrast agents are used in imaging the soft tissues of the body with X-rays. More recently, substantial efforts have been made to exploit deeply penetrating, low frequency (e.g., infrared) wavelengths for non-invasively imaging living tissue. These techniques could be used in principle not only to discern different tissues, but also as sensors to detect changes in tissue properties. The benefits of non-ionizing, deeply penetrating wavelengths, however, are compromised by a lack of suitable contrast in translucent or transparent organic media.

The difficulty of obtaining adequate optical contrast using current imaging techniques arises from two major limitations: the restriction of instrument sensitivity to amplitude variations and the inherently limited signal-to-noise ratio of DC or low frequency measurements. The first issue has been addressed, for example, by Zernicke, who used optical processing techniques to render the phase changes of light passing through varying materials visible ("phase contrast microscopy"). However, these techniques are limited in their sensitivity as well. Because the measurements are made at DC, the received signal cannot be profitably amplified to distinguish between materials that have very similar optical properties.

The problem of noise susceptibility in low-frequency measurements can be addressed with

synchronous detection. The DC signal of interest is AC modulated into a region of relatively low instrumentation noise. Once in this region, the signal can be profitably amplified and small variations resolved. The modulation of the DC signal can be accomplished by the application of external stress, electric fields, and magnetic fields, which modulate the optical polarization properties of a material.

1.2 Goal of Thesis

This goal of this thesis is to enhance optical contrast in transparent or translucent materials by combining an externally-modulated optical property with synchronous AC detection. The AC modulation of the optical property of interest will shift the material's optical information into a low-noise region of an imaging instrument's spectrum. The optical properties of most materials can be altered with magnetic fields. Specifically, the polarization state of light passing through a material may be *externally* controlled by an applied magnetic field, i.e. the Faraday effect. The frequency of an applied *alternating* magnetic field can be adjusted to maximize the signal strength of the transmitted light's polarization state with respect to noise. The technique could result in unprecedented sensitivity to a material's optical properties.

1.3 Thesis Outline

This thesis will explore the use of the Faraday effect as a contrast agent in optical imaging systems. Chapter 2 provides a brief overview of existing phase imaging modalities and their limitations. The possible use of stress, electric, and magnetic fields is then explored, and the Faraday effect is found to be the most practical option for external modulation of optical properties. Chapter 3 provides develops the origin of the Faraday effect and addresses the practical issues of using magnetic fields as a contrast mechanism. Chapter 4 describes the implementation of the Faraday effect contrast imaging system, and Chapter 5 presents the results and future directions for this technique. The thesis is summarized in Chapter 6.

Chapter 2

Overview of Optical Imaging Techniques

2.1 Introduction

The need to image and identify transparent and semi-transparent objects has led to several techniques for improving contrast in microscopy. As described in [24], staining techniques were first developed in the nineteenth century to address the fact that "under ordinary microscope illumination unstained cells and tissues are practically invisible." In order to fully benefit from staining, fixation techniques were also introduced to help expedite the placement of stains in prescribed regions of the tissue[24]. A problem with these staining and fixation techniques, however, was that they usually destroy the life-process under study [11], leading to "artifacts" in the data that complicate the interpretation of an image. The problems of artificial staining can be addressed by rendering alternative "invisible" properties of light visible, specifically the phase or polarization of the light wave.

This chapter provides an overview of existing non-invasive phase techniques and how their limitations are addressed through external modulation of optical properties. The phase contrast and interference microscopes are discussed to illuminate the concepts that govern their utility. Their limitations are then discussed, and alternative polarization techniques that allow for *external* modulation of material properties are explored. The primary advantage of external modulation is that optical phenomena can be synchronously detected. Synchronous detection

can improve the signal-to-noise ratio for the optical measurement and help differentiate similar materials. It will be shown that, of many possible modulation techniques, the Faraday effect provides significant benefits for improving the imaging and identification of transparent materials. A brief discussion of related Faraday effect microscopy for the imaging of magnetic domains will also be discussed to distinguish it from the technique presented here.

2.2 Phase Imaging Techniques

2.2.1 Background

Phase contrast [PCM] and interference microscopy provide contrast in transparent materials without the need for external staining. Although most transparent objects provide little amplitude modulation of light, their refractive properties effect the phase of a light wave. This phase effect is invisible to the human eye and all other intensity detectors, and must therefore be translated into an amplitude-modulated image. The phase contrast microscope and interference microscope provide a means of accomplishing this translation.

2.2.2 Principles of Phase Contrast Microscopy

Although transparent objects provide limited modulation to light, they can have a dramatic effect on the phase properties of a wave. These phase properties arise from variations in the sample's refractive indices along the optical path. Recalling that the speed of light in a material is

$$v = \frac{c}{n},$$

where c is the speed of light in vacuum, the variations in a material's index of refraction, n result in variations in the speed of the light wave while passing through a material. Upon exiting a material of length l, the net phase of the light wave is

$$\phi = \frac{2\pi l n}{\lambda},$$

where λ is the wavelength of the light in vacuum. The phase difference between this wave and a reference with refraction index n_o is simply

$$\Delta\phi = \frac{2\pi l}{\lambda}(n - n_o) = \frac{2\pi l}{\lambda}\Delta n.$$

The phase variation can be used as a contrast mechanism. Figure 2-1 illustrates this concept for a light wave passing through both a stained and unstained cellular structure. The stained material attenuates the wave amplitude in regions of absorption, and renders them visible. The unstained cell provides little amplitude variation of the light waves, but the phase is modulated throughout the cellular structure. The phase modulation of the unstained cell is similar to the absorption modulation of the stained cell; the problem is rendering the phase modulation visible.

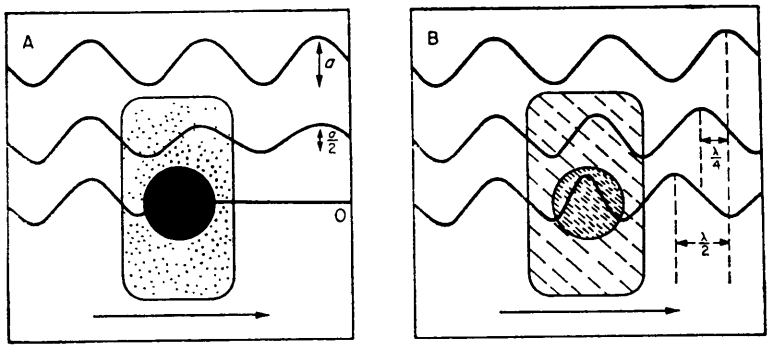

Fig. 1 A—The reduction in amplitude of waves of light passing through a stained cell. The waves passing through the full thickness of stained cytoplasm have been reduced to half the background amplitude and those passing through the centre of a very heavily stained circular-shaped inclusion have been completely absorbed and emerge with an amplitude of zero.
B—Retardations in phase in waves of light passing through a transparent living cell mounted in saline. The waves passing through the full thickness of the cytoplasm have been retarded by $\frac{1}{4}\lambda$ and those passing through the full thickness of a more highly refractile inclusion and some cytoplasm have been retarded by $\frac{1}{2}\lambda$.

Figure 2-1: Illustration of Absorption and Refractory Properties of Materials. Figure from [24].

Zernicke realized that the variable phase offsets of plane waves passing through transparent materials could be transformed into amplitude-modulated images using spatial filtering [30]. The method of spatial filtering is derived from the phase relationships between the scattered and unperturbed light in a sample.

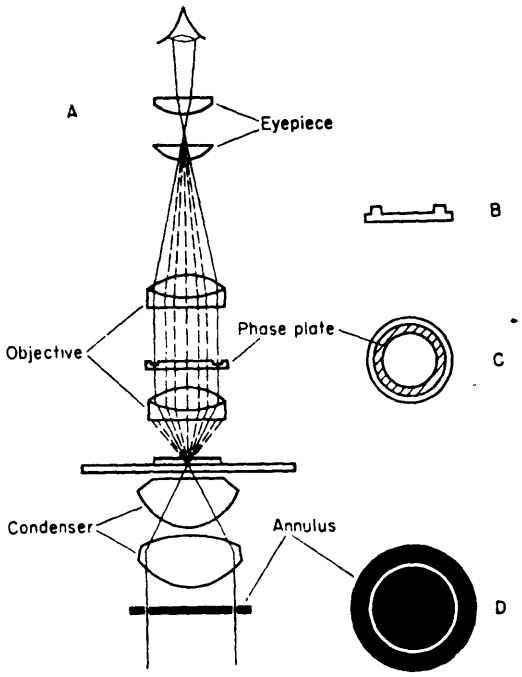

Fig. 3 A—The paths taken by the directly transmitted light (continuous lines) and the light diffracted by an object (broken lines) through an ordinary Zernike phase contrast microscope, showing sectional views of a ring-shaped sub-stage annulus in the front focal plane of the condenser and a ring-shaped +ve phase plate in the back focal plane of the objective. (The pencil of rays entering the eye from the Huygenian eyepiece has been drawn so that it diverges slightly instead of being parallel, as normally drawn in these optical diagrams, because it has been very recently established by Baker (1966) that the human eye is normally almost always focused for near vision when looking down a microscope.)

B—Sectional view of a −ve phase plate which could be substituted for the +ve phase plate shown in A.

C—Plan view of phase plate.

D—Plan view of sub-stage annulus.

Figure 2-2: System Diagram for Phase Contrast Microscope. Figure from [24].

A wave passing through a material gains a phase shift $\Delta\phi$ due to the index of refraction. The resulting light wave,

$$\exp(j(kx - \omega t + \Delta\phi)),$$

can be approximated as

$$[1 + j\Delta\phi]\exp(j(kx - \omega t),$$

if the phase offset $\Delta\phi$ is small. This equation can be interpreted as the superposition of the incident plane wave,

$$\exp(j(kx - \omega t)),$$

and a scattered wave,

$$j\Delta\phi(\exp(j(kx - \omega t)),$$

containing information about the material's constituents[5]. In addition to being small, the scattered wave is shifted by ninety degrees with respect to the original wave. The two waves therefore cannot interfere with each other, and the scattered wave's effect on the observed intensity,

$$I_{obs} \approx 1 + (\Delta\phi)^2,$$

is second order and essentially invisible.

Shifting the diffracted wave an additional ninety degrees allows the scattered wave to interfere with incident plane wave. The phase modulation is then a *first order* perturbation of the observed intensity,

$$I_{obs} \approx 1 + (\Delta\phi),$$

and the effects of the scattered wave are more distinguishable. Figure 2-2 illustrates a microscope that provides the proper phase shift to the scattered wave. An annulus is placed in the light path between the source and condenser which restricts the illumination of the specimen to a finite solid angle. After passing through the sample, the unperturbed light exits the sample in a cone defined by the angle of incidence. The scattered light, however, is diffracted outside of this cone. By placing a phase plate into the path of the light, the unperturbed light wave passes through a thin region of the plate and the refracted light wave passes through a thicker

region(see part c of Figure 2-2). If the optical distance between the two regions is adjusted appropriately, the refracted wave can be shifted an additional quarter-wave length, and the two waves can interfere.

This elegant solution provides images of specimens that rivals those used with stains, but with no chemical or mechanical interference. In addition, the physical basis for the microscope allows for quantitative measurements of the cell properties, specifically the concentration of proteins and other cytological chemicals [24].

2.2.3 Principles of Interference Microscopy

The interference microscope is similar to the PCM in that is converts phase offsets caused by the refractive indices of materials into visible amplitude modulations. Instead of interfering the transmitted and refracted waves passing through a sample, the interference microscope splits the beam, passes one leg through the sample, and recombines this beam with the reference. This setup is quite similar to the Michelson interferometer, with the modification being the placement of a sample (instead of "ether") along one optical path. The principles of operation for the interference microscope are very similar to those of the PCM, and will not be elaborated here.

2.2.4 Limitations of Phase Contrast and Interference Microscopy

The phase contrast and interference microscopes help render phase changes visible, and eliminate the need for external staining. However, the refractive properties of many biological and chemical substances are often very similar, making it difficult to identify the precise material structure of a specimen. Table 2.1 illustrates the similarity of biological refractive properties. The refractive indices shown indicate how much the index of refraction increases for each 1g addition of material to solution. As an example, the difference between sucrose and glucose is in the third decimal point, which can make them hard to uniquely identify. Although the phase contrast technique is useful to tell that some material is present, the similarity in refraction indices prevent the technique from identifying precisely the chemical constituents[24]. Simple amplification of the output signals does not solve the problem because of large amounts of drift assosciated with a DC measurement.

The significant drawback of existing optical methods such as phase contrast and interference microscopy is that they are inherently DC measurements; the properties of the cellular material are static, as is the imaging system. Low frequency noise will therefore limit the accuracy of the measurement if the signal from the detector is simply passed through a DC amplifier. This noise, generally referred to as drift or 1/F-noise, "can be introduced by long-term power fluctuations, changes in component values, temperature drifts, and other sources whose exact nature is poorly understood.[10]" The name "1/F" arises from the fact that the spectral envelop of the drift noise varies roughly as 1/f, where f is the frequency in hertz [10, 13, 9]. Drift noise in the light source, detector, and electronics will all act to limit the accuracy of the intensity measurement, and the ability to accurately resolve the small differences in materials will be compromised.

A technique that circumvents the 1/F noise is synchronous detection. Synchronous detection modulates the DC signal of interest at a frequency above the 1/F noise for a system. This allows for a significant increase in the resolution of small signal variations[10]. In order to implement synchronous detection, however, the signal must have some means of being modulated externally. Since the optical properties of a material are of interest in this thesis, we seek a method of externally modulating a particular optical property and synchronously detecting the intensity of light. Several methods of external modulation are available, and are discussed in the next section.

Material	Specific Refraction Increment
Bovine plasma albumin	0.00182
Human serum albumin	0.001862
Human serum globulin	0.00186
Human haemoglobin	0.001942
Glycine	0.00179
Alanine	0.00171
Valine	0.00175
Tryptophane	0.0025
DNA	0.00181
RNA	0.00194
Sucrose	0.00141
Glucose	0.00143
Starch	0.00133
NaCl	0.00163
KCl	0.00115
CaCl2	0.0021

Table 2.1: Specific Refraction Increments, from [24].

2.3 External Modulation Schemes

The use of external modulation techniques has the promise of dramatically improving the sensitivity of optical instrumentation by pushing the signal into a region of extremely low noise. Several options for modulating the material's optical properties are discussed in this section. These techniques range from the application of mechanical stress to the immersion of the sample in electric and magnetic fields. In all cases, the result is the modulation of the polarization state of the light wave traversing the material. Consideration of the practical implementations of these approaches indicates that the Faraday effect is most promising for imaging applications.

2.3.1 Photoelasticity

Brewster discovered that isotropic substances can be transformed into birefringent optical materials by the application of mechanical stress [11]. The optical axis is aligned with the axis of this applied stress, and is linearly proportional to its magnitude. This effect has found numerous applications in studying the stresses of transparent objects, ranging from telescope lenses to car windshields [11].

The difficulty of applying this effect in practical imaging systems is the challenge of applying the stress with any degree of homogeneity. In addition, the microscopic application of stresses to biological cells or tissues is nearly impossible. Although an interesting technique, it is inappropriate for modulating the optical properties of transparent microscopic, and most macroscopic, materials.

2.3.2 Electro-optical Effects

Kerr discovered that the application of an electric field across an isotropic transparent substance would induce birefringence [2]. The new optical axes are oriented relative to the applied electric field, each with their own index of refraction. The difference in the magnitude of these refraction indices are found to be quadratic,

$$\Delta n = \lambda_o K E^2,$$

where K (Kerr constant) is a proportionality factor that varies between materials. This phenomena is attributed to the alignment of anisotropic molecules with the applied field [11].

Another electro-optical mechanism to modulate the material's properties is the Pockel's effect[8]. The Pockel's effect varies linearly with the applied electric field. It is restricted, however, to crystals that lack a specific symmetry; that is the "lack of a central point through which every atom can be reflected into an identical atom. [11]" This effect is not seen in liquids and most crystals, giving it very limited utility as a general contrast mechanism.

Although the Kerr effect, and to a lesser extent Pockel's effect, provide a means to modulate the material's optical properties externally, they both suffer from a fundamental limitation in terms of the modulation frequency. The materials of interest in this thesis are fairly conductive, often with conductivities in the range of 1-10 mhos/m. In the presence of an external electric field, the free charges can move so as to shield the material from the applied field. The speed with which the material can respond is regulated by the dielectric relaxation time,

$$\tau = \epsilon/\sigma,$$

which provides a lower bound on the modulation frequency required to maintain a significant electric field through a material. In substances of interest for this thesis, the dielectric relaxation time is on the order of 0.1-1 ns. Frequency modulations below the tens of megahertz range will therefore be completely ineffective at modulating the optical properties of a material. Primarily for this reason, the use of electro-optical effects to modulate the optical properties of materials is not a practical choice.

2.3.3 Magneto-optical Effects

A magnetic field's behavior is governed by a time constant similar to dielectric relaxation, but the interpretation is different. The characteristic magnetic diffusion time constant,

$$\tau_m = \frac{\mu\sigma d^2}{\pi^2},$$

for materials identical to those used in the previous analysis, and with dimension $d \approx 0.1cm$, in on the order of 1 ps. This constant denotes the amount of time it takes for a magnetic field

to diffuse into a conducting material. It puts an *upper* bound on the modulation frequency of interest, and for the materials under study in this thesis it is well beyond that required for significant improvement of the signal-to-noise ratio.

The use of magnetic fields to modulate the material optical properties suggests two possible phenomena; the Faraday effect [4] and the Cotton-Mouton effect [11]. The Faraday effect is the rotation of the plane of polarization along the axis of an applied magnetic field. The rotation angle is a linear relationship,

$$\phi = VB_o l,$$

between the applied field, B_o, the length of traversal, l, and a proportionality constant, V. The Verdet constant is a property of the material [16, 11, 18]. The Cotton-Mouton effect is the induction of birefringence when light traverses perpendicular to the axis of an applied magnetic field. The Cotton-Mouton effect is much weaker than the Faraday effect, and will not be considered more here.

The Faraday effect is the most promising optical modulation technique for employing synchronous detection schemes. It relies on an applied magnetic field, which allows for practical modulation due to the extremely fast magnetic diffusion time constants of materials of interest. In addition, the Verdet constant shows a large variation across materials, which will help differentiate the constituents of a sample.

2.4 Related Faraday Imaging Techniques

This section discusses some related imaging applications of the Faraday effect. The Faraday effect and magneto-optic Kerr effect[1] are used extensively in the imaging of domain patterns in magnetic media[6, 21, 28]. An example of the this work is illustrated by the imaged domain pattern in Figure 2-3, where the bar reference is $10\mu m$ in length. The application of the Faraday effect has also progressed to scanning tunneling microscopy[22], with nm-level resolution of magnetic domains.

The application of an *external* magnetic field to an inherently non-magnetic material for the creation of optical contrast, however, is a new concept. The advantages of this approach over

[1]Rotation of the plane of polarization upon reflection from a magnetic surface.

existing optical instrumentation is two-fold: the optical properties are externally modulated and may be selectively enhanced with synchronous detection, and the range in the Verdet constant among materials is generally more significant than the variation among the indices of refraction. A thorough theoretical understanding of the Faraday effect is needed to understand the basis for this large variation and to insure that the linear relationship still holds in the presence of an oscillating magnetic field. The next chapter provides a theoretical overview of the propagation of light through matter, with particular emphasis on the rotation of the plane of polarization in optically-active materials.

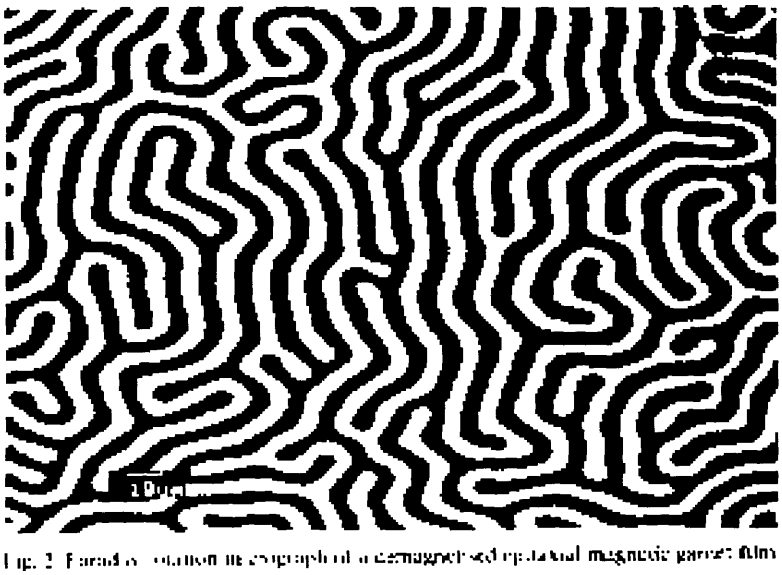

Figure 2-3: Imaging of Domain Patterns with Kerr/Faraday Microscope; from [28].

Chapter 3

Theoretical Development of the Faraday Effect

3.1 Introduction

Chapter 2 introduced the strategy of modulating optical properties in order to improve sensitivity to small material variations. The use of the Faraday effect was found promising because of the effective penetration of the magnetic field into a sample and the wide range in Verdet constants. This chapter serves as a detailed development of the Faraday effect in materials. Through the use of Maxwell's equations and the susceptibility tensor, the effect of an external magnetic field on the optical characteristics of a homogeneous material will be better understood. Although this development is an overview of more thorough treatments of the subject, most notably [7], it is designed to briefly convey the practical considerations of using the Faraday effect as an optical modulation technique.

3.2 Electromagnetic Wave Propagation through a Material

3.2.1 Wave Propagation from Maxwell's Equations

This section develops the equations for electromagnetic wave propagation necessary to understand the Faraday effect. Maxwell's equations form the basis for understanding light propaga-

tion through matter. The equations for electromagnetic fields are

$$\vec{\nabla} \times \vec{E} = -\frac{\partial \vec{B}}{\partial t}$$

$$\vec{\nabla} \times \vec{H} = \vec{J} + \frac{\partial D}{\partial t}$$

$$\vec{\nabla} \cdot \vec{D} = \rho$$

$$\vec{\nabla} \cdot \vec{B} = 0$$

where the materials of interest in this development are assumed to have no significant magnetization ($\vec{M} = 0$). The interaction between the electric field and a material is incorporated in the displacement field, $\vec{D}$. The displacement field,

$$\vec{D} = \epsilon_o \vec{E} + \vec{P},$$

is defined as the superposition of the applied electric field $\vec{E}$ and the field due to material polarization $\vec{P}$. The interactions of the electric field, $\vec{E}$, with a material are then implicit in the susceptibility tensor, χ, that relates the applied electric field with the resulting polarization,

$$\vec{P} = \chi \epsilon_o \vec{E},$$

assuming a linear material[1]. Manipulation of the four basic equations decouples the electric and magnetic fields, and yields a general wave equation for the electric field,

$$\nabla^2 \vec{E} + \frac{1}{c^2} \frac{\partial^2 \vec{E}}{\partial t^2} = -\mu_o \frac{\partial^2 \vec{P}}{\partial t^2} - \mu_o \frac{\partial \vec{J}}{\partial t},$$

where the speed of light in vacuum,

$$c = \frac{1}{\sqrt{\mu_o \epsilon_o}}$$

[1] At the field strengths in this thesis this in an excellent approximation.

has been substituted. This expression can be interpreted as the standard wave equation for a vector field (left hand side), with two source terms (right hand side) [7]. The expression

$$-\mu_o \frac{\partial^2 \vec{P}}{\partial t^2}$$

represents the effects of the polarization properties of material, while the expression

$$-\mu_o \frac{\partial \vec{J}}{\partial t}$$

represents the flow of free charges in the material.

In analyzing a specific physical problem it is often useful to compare the relative magnitude of these two source terms. Comparing their relative scales,

$$\epsilon_o \omega \chi E \Leftrightarrow \sigma E,$$

it is clear that a time constant,

$$\tau_d = \omega^{-1} = (\frac{\sigma}{\chi \epsilon_o})^{-1} \approx (\frac{\sigma}{\epsilon})^{-1},$$

delineates two limits of analysis. This time constant is the dielectric relaxation time previously discussed in Chapter 2. For electric field variations occurring on time scales below τ_d, free charge movement is the predominant source term. Likewise, the polarization properties of a material dominate behavior for electric field variations that occur much faster than τ_d. The materials of interest in this thesis, suspended in physiological saline for example, have a dieletric relaxation time on the order of nanoseconds. The electromagnetic waves generally used in imaging and spectroscopy lie in the optical range between 300 and 700 nm, resulting in temporal variations on the order of femtoseconds. This time scale is significantly above the dielectric time constant for materials of interest. The free charge source term can the therefore be suppressed, resulting in a simplified equation for the electric field,

$$\nabla^2 \vec{E} + \frac{1}{c^2} \frac{\partial^2 \vec{E}}{\partial t^2} \approx -\mu_o \frac{\partial^2 \vec{P}}{\partial t^2}.$$

Recalling the definition of a material's polarization,

$$\vec{P} = \epsilon_o \chi \vec{E},$$

the wave equation takes the form

$$-\nabla^2 \vec{E} + \frac{1}{c^2}\frac{\partial^2 \vec{E}}{\partial t^2} = -\frac{1}{c^2}\frac{\partial^2 \chi \vec{E}}{\partial t^2}$$

$$\nabla^2 \vec{E} = \frac{1}{c^2}(1+\chi)\frac{\partial^2 \vec{E}}{\partial t^2}.$$

This equation illustrates that the details of electromagnetic wave propagation in a material are embedded within the susceptibility tensor χ.

3.3 Susceptibility Tensor for Homogeneous Materials

This section explores the origin of electric susceptibility in a homogeneous material and it's effect on wave propagation.

3.3.1 Wave-Electron Interactions

The origin of susceptibility lies in the interaction of light with the bound electrons of an atom. A useful classical model for understanding this interaction is the damped mass-spring oscillator [5, 7, 15] (See Figure 3-1). The mass term, m, represents the "effective" mass of the electron, the spring constant, k, is the electrostatic Coloumb potential between the electron and nucleus, and the damping coefficient, γ, is derived from radiation damping[2]. Using this model, the equation of motion for the electron is then

$$m\ddot{x} + \gamma m\dot{x} + kx = F_x.$$

When driven by an electromagnetic wave the force, F, is composed of both electric and magnetic components. However, the magnitude of the electrical force is dominant, and the

[2]The details of the damping term due to radiation is complex, and is beyond the scope of the analysis. Far from an optical resonance it is very small and can be ignored.

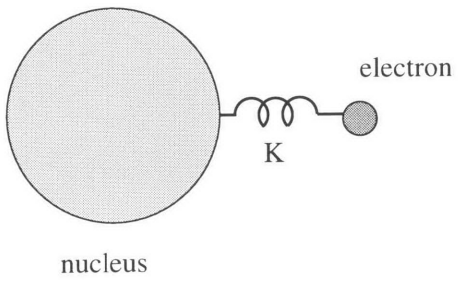

Figure 3-1: Simple Model of Electron as Mass-Spring System.

magnetic field is omitted from further analysis[5, 7, 15]. The electric field from the light wave is

$$\vec{E} = E \exp(-j\omega t)\hat{x},$$

and the resulting steady-state magnitude of the electron's motion is given by

$$-m\omega^2 x - \gamma\omega j x + kx = qE.$$

Defining the resonant frequency for the system,

$$\omega_o = \sqrt{\frac{k}{m}},$$

the complex electron displacement is found to be

$$x_o = \frac{qE}{m} \frac{1}{\omega_o^2 - \omega^2 - j\omega\gamma}.$$

Substitution of the physical definition of polarization, $P = Nqx_o$, gives the susceptibility

$$\chi = \frac{P}{\epsilon_o E} = \frac{Nq^2}{m\epsilon_o} \frac{1}{\omega_o^2 - \omega^2 - j\omega\gamma},$$

where N represents the density of atoms in the material.

3.3.2 Susceptibility Effects on Wave Propagation

Although the susceptibility for a homogeneous material was derived using a simple model, it does demonstrate many of the properties that are observed in homogeneous transparent materials. The damped harmonic oscillator model has no dependence on the direction of the applied field, and the three diagonal elements of the susceptibility tensor

$$\chi = \begin{pmatrix} \chi & 0 & 0 \\ 0 & \chi & 0 \\ 0 & 0 & \chi \end{pmatrix},$$

are the same expression,

$$\chi = \frac{P}{\epsilon_o E} = \frac{Nq^2}{m\epsilon_o} \frac{1}{\omega_o^2 - \omega^2 - j\omega\gamma}.$$

The lack of off-diagonal components insures that no coupling of fields exists between the different axes of the material. Direct substitution of the susceptibility tensor into the wave equation yields the equation of propagation for an electromagnetic wave traversing a homogeneous material,

$$\nabla^2 \vec{E} = \frac{1}{c^2}(1 + \frac{Nq^2}{m\epsilon_o} \frac{1}{\omega_o^2 - \omega^2 - j\omega\gamma}) \frac{\partial^2 \vec{E}}{\partial t^2}.$$

The solution of this differential equation is an electric field,

$$\vec{E} = E \exp(j(\vec{k} \cdot \vec{r} - \omega t)),$$

that propagates with a wavevector $\vec{k}$ obeying the dispersion relation,

$$k^2 = \frac{\omega^2}{c^2}(1 + \frac{Nq^2}{m\epsilon_o} \frac{1}{\omega_o^2 - \omega^2 - j\omega\gamma}).$$

A better understanding of the material's dispersion characteristics is obtained by analyzing the index of refraction. The index of refraction for a homogeneous material is defined by

$$n^2 = \frac{c^2k^2}{\omega^2} = (1 + \frac{Nq^2}{m\epsilon_o}\frac{1}{\omega_o^2 - \omega^2 - j\omega\gamma}),$$

and is a complex function of frequency. The real part of the index of refraction is plotted as a function of frequency in Figure 3-2 (Three different damping ratios are plotted, $\gamma = 0.1, 0.2, 0.3$). Recalling that the speed of light in a material is

$$v(\omega) = \frac{c}{n(\omega)},$$

the plot of the index of refraction illustrates that higher frequency (lower wavelength) light travels slower through the material below an optical resonance ($f = 5$). This effect causes *dispersion* of waves propagating through a material; the effects of this ranging from pulse-broadening of light beams to the colors observed from a prism. The real part of index of refraction is also important for phase contrast imaging. The variation in the index of refraction as a result of susceptibility differences between materials can lead to observable phase offsets. Recall from Chapter 2 that the net phase after traversing a material of length l is

$$\Phi = \frac{2\pi ln}{\lambda},$$

where λ is the wavelength of light in vacuum. Differences in n or l will create variations in Φ which may be observed with a phase sensitive instrument.

The imaginary component of the index of refraction represents the absorption spectra of a material, as illustrated in Figure 3-3 (Once again, three different damping ratios are plotted, $\gamma = 0.1, 0.2, 0.3$). The spectrographic profile of a material is unique[27], and can serve as a useful fingerprint for identification. This observation forms the basis for spectrometers in use today.

Although a homogeneous material does have identifying characteristics such as absorption spectra and phase offsets, these defining traits are often hard to discern for transparent materials[24]. As developed in Chapter 2, an alternative scheme is needed that can modulate

the optical properties externally and thereby improve resolution through synchronous detection. The external modulation of optical properties can be accomplished with a magnetic field.

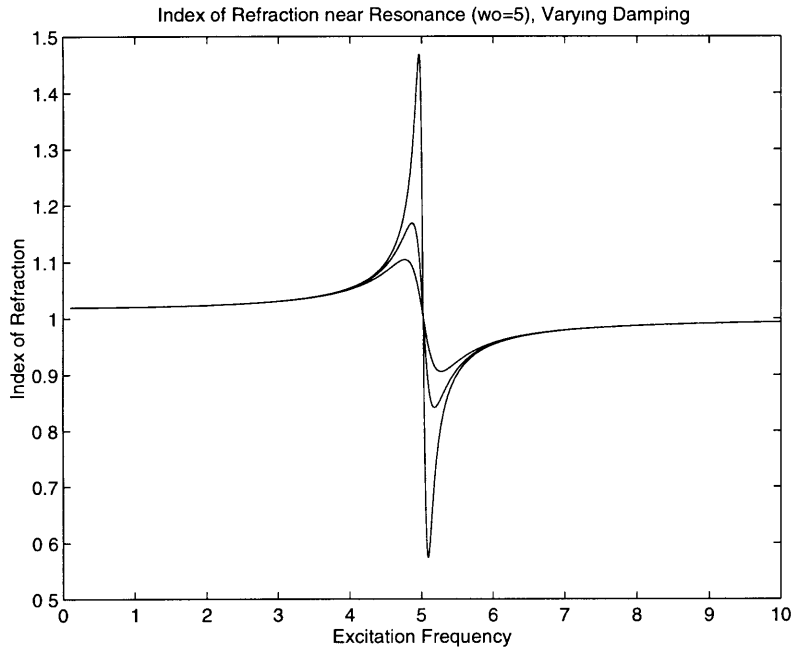

Figure 3-2: Index of Refraction near Resonance.

3.4 External Manipulation of the Susceptibility Tensor

This section explores the effect of an external magnetic field on the optical properties of a material. The susceptibility tensor is generally an inherent property of a homogeneous material; however, the application of a strong magnetic field can dramatically change the tensor structure of a homogeneous material. This effect allows for external modulation of optical properties.

In the previous section, a homogeneous material's susceptibility was derived by treating the electron as a damped harmonic oscillator. The equation of motion was

$$m\ddot{x} + \gamma m\dot{x} + kx = qE_x,$$

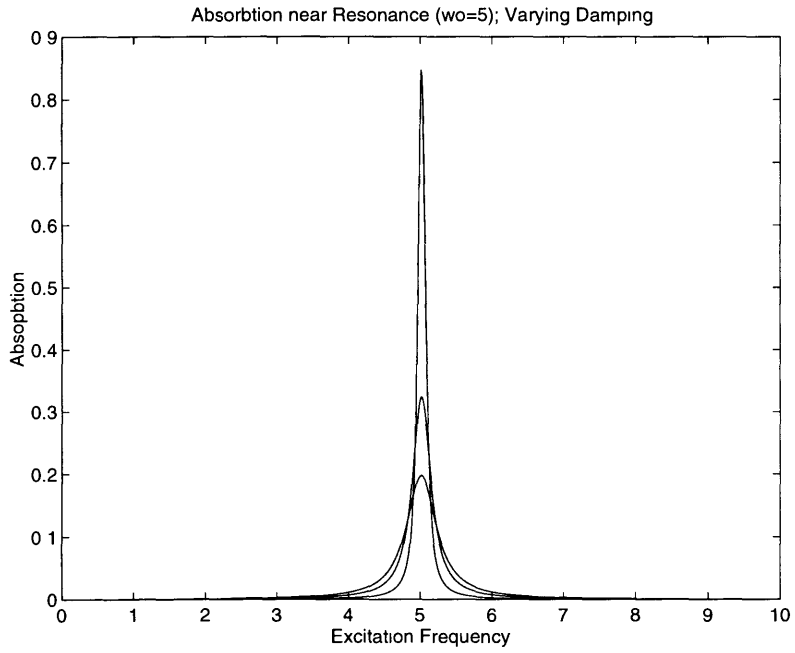

Figure 3-3: Absorbtion Spectrum near Resonance.

where the magnetic field of the propagating wave is small enough to be neglected. Upon application of a strong external magnetic field, $B_o\hat{z}$, the effects of the magnetic field must also be considered. The equation of motion for the electron is then of the form

$$m\frac{\partial^2\vec{r}}{\partial t^2} + \gamma m\frac{\partial\vec{r}}{\partial t} + k\vec{r} = -q\vec{E} - \frac{q}{c}(\vec{v}\times\vec{B_o}),$$

where the position vector $\vec{r} = x\hat{x} + y\hat{y} + z\hat{z}$. To help simplify analysis, the frequency of the electromagnetic wave is assumed far enough from resonance that the damping term may be neglected [7]. In addition, the wave propagates parallel to the applied magnetic field.

Expanding the equation of motion for sinusoidal field modulations, the equations governing the magnitude of electron motion in the x-y plane are found to be:

$$(-m\omega^2 + k)x = -qE_x + \frac{j\omega e}{c}B_o y$$

$$(-m\omega^2 + k)y = -qE_y + \frac{j\omega e}{c}B_o x.$$

The magnitude of displacement of an electron is then found with further manipulation:

$$x = \frac{1}{[(\omega_o^2 - \omega^2)^2 + \omega^2\omega_c^2]}[\frac{qE_x}{m}(\omega_o^2 - \omega^2) + \frac{j\omega\omega_c eE_y}{m}]$$

$$y = \frac{1}{[(\omega_o^2 - \omega^2)^2 + \omega^2\omega_c^2]}[\frac{qE_y}{m}(\omega_o^2 - \omega^2) - \frac{j\omega\omega_c eE_x}{m}],$$

where the cyclotron frequency

$$\omega_c = \frac{eB_o}{m}$$

has been substituted into the expressions. Substitution of these equations for the net electron displacement into the polarization equation yields the susceptibility tensor[7],

$$\chi = \begin{pmatrix} \chi_{11} & j\chi_{12} & 0 \\ -j\chi_{12} & \chi_{11} & 0 \\ 0 & 0 & \chi_{33} \end{pmatrix},$$

with matrix components

$$\chi_{11} = \frac{Ne^2}{m\epsilon_o}[\frac{\omega_o^2 - \omega^2}{(\omega_o^2 - \omega^2)^2 + \omega^2\omega_c^2}]$$

$$\chi_{12} = \frac{Ne^2}{m\epsilon_o}[\frac{\omega\omega_c}{(\omega_o^2 - \omega^2)^2 + \omega^2\omega_c^2}]$$

$$\chi_{33} = \frac{Ne^2}{m\epsilon_o}[\frac{1}{(\omega_o^2 - \omega^2)^2}].$$

The new susceptibility tensor has off-diagonal terms that are proportional to the applied magnetic field. The tensor component, χ_{12}, serves to couple a propagating electric field polarized in the $\vec{x}$ direction into the $\vec{y}$ direction, and vice-versa. The net effect of the magnetic field is to induce the rotation of the plane of polarization as the wave propagates through the material. This behavior is the property of an optically active material, which is developed fully in the next section.

3.5 Susceptibility Tensor for Optically-Active Materials

This section explores the properties of an optically-active material. Specifically, the connection between the off-diagonal components of the susceptibility tensor and the rotation of the light's plane of polarization is established.

3.5.1 Form of the Susceptibility Tensor

It can be shown that the general form of the susceptibility tensor for an optically-active material is

$$\chi = \begin{pmatrix} \chi_{11} & j\chi_{12} & 0 \\ -j\chi_{12} & \chi_{11} & 0 \\ 0 & 0 & \chi_{33} \end{pmatrix},$$

where the off-diagonal elements are the complex conjugates of one-another[7]. Substitution of this tensor into the wave equation,

$$-\nabla^2\vec{E} + \frac{1}{c^2}\frac{\partial^2\vec{E}}{\partial t^2} = -\frac{1}{c^2}\frac{\partial^2\chi\vec{E}}{\partial t^2},$$

yields a set of dispersion relations for propagating electromagnetic waves. These dispersion relations,

$$k_\pm = \frac{\omega}{c}\sqrt{1+\chi_{11}\pm\chi_{12}}$$

have corresponding indices of refraction defined by,

$$n_\pm = \frac{ck}{\omega} = \sqrt{1+\chi_{11}\pm\chi_{12}}.$$

Substitution of the dispersion relationships back into the wave equation yields the eigenvectors for the system. The eigenvectors are found to be two propagating waves with components constrained by

$$E_x = \pm jE_y.$$

This constraint is physically interpreted as two circularly-polarized transverse waves[3]. The fact that the index of refraction is dependent on the "handedness" of the wave indicates that their relative speed of propagation through a material will be different. This observation forms the basis for the rotation of the polarization axis by an optically active material.

3.5.2 Rotation of Plane of Polarization

The difference in the index of refraction between two circularly-polarized waves results in the rotation of the plane of polarization. A linearly polarized light wave may be conceptualized as the sum of two circularly polarized waves, as illustrated in Figure 3-4. When a linearly-polarized wave enters an optically active material, the circularly polarized waves propagate independently at different velocities. Upon exiting the material, the circularly polarized waves are still equal

[3]Looking along the direction of wave propagation, the electric field vector traces a circle about the propagation axis.

in magnitude, but now have a relative phase shift of

$$\Phi = (n_l - n_r)\frac{\pi l}{\lambda},$$

where l is the length of propagation through the material, λ is the wavelength of light, and n_l, n_r are the respective indices of refraction for left and right-handed polarized waves. The net effect of the phase shift is that upon exiting the material, the resulting wave is still linearly polarized, but rotated by an angle $\Phi/2$ about the axis of the applied magnetic field (Figure 3-5). Using the relationship between the index of refraction and the susceptibility, the rotation angle of the polarization vector is found to be

$$\Phi = \frac{\pi l}{\lambda}\frac{\chi_{12}}{\sqrt{1+\chi_{11}}}.$$

This expression is the basis for the Verdet constant [7].

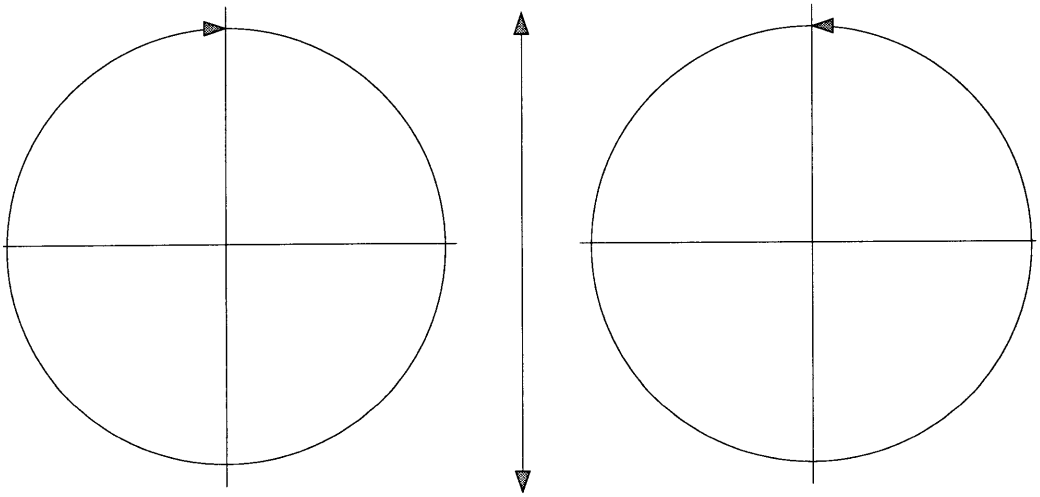

Figure 3-4: Linearly Polarized Wave is Sum of Two Circularly-polarized Waves.

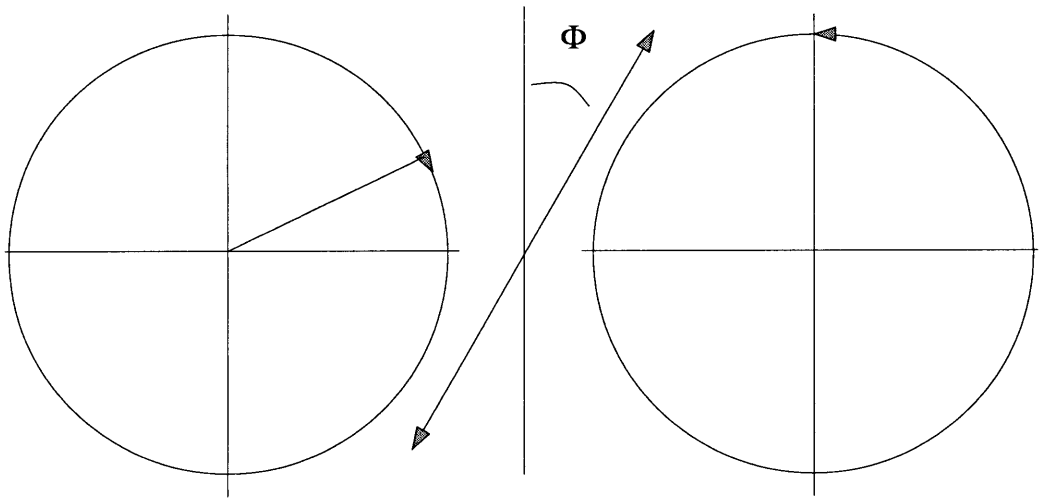

Figure 3-5: Net Polarization Vector after Propagation through Active Material.

3.6 The Verdet Constant

This section determines the expression for the Verdet constant and how it relates to a material's properties. The expression for the Verdet constant is also compared with that of the index of refraction.

3.6.1 The Origin of the Verdet Constant

The Faraday effect is generally defined by the simple formula

$$\Phi = VB_o l.$$

Direct substitution of the tensor elements, χ_{12}, χ_{11}, into the expression for the rotation angle

$$\Phi = \frac{\pi l}{\lambda} \frac{\chi_{12}}{\sqrt{1+\chi_{11}}} [7],$$

yields the Verdet constant[7]

$$V = \frac{\pi N q^3}{\lambda m^2 \epsilon_o} \frac{\omega}{(\omega_o^2 - \omega^2)^2}.$$

The Verdet constant is seen to have direct dependencies on the effective mass of the electron, m, the resonant frequency for the "mass-spring" system, ω_o, and the number of electrons, N. These dependencies result in a unique fingerprint for different materials as well as a large range of Verdet constants, as Table 3.6.2 shows.

3.6.2 Comparison with the Index of Refraction

Recall that the index of refraction for a homogeneous material is found to be

$$n^2 = \frac{c^2k^2}{\omega^2} = (1 + \frac{Nq^2}{m\epsilon_o}\frac{1}{\omega_o^2 - \omega^2 - j\omega\gamma}).$$

For transparent materials

$$\frac{Ne^2}{m\epsilon_o}\frac{1}{\omega_o^2 - \omega^2 - j\omega\gamma}) \approx 1,$$

and the spread in the indices of refraction is limited to a factor of two, as shown in Figure 3-6[11]. It can therefore be difficult to observe small variations in the material constituents.

The Faraday effect, however, is a *differential* measurement,

$$\Phi = (n_l - n_r)\frac{\pi l}{\lambda}.$$

This results in the Verdet constant containing only terms from the material properties. This fact helps accentuate a material's effects on the propagating electromagnetic wave and uniquely define it based on the observed Verdet constant.

A trait common to both the Verdet constant and the index of refraction is a dependence on wavelength. As the frequency of the electromagnetic wave approaches that of the optical resonance for the system, ω_o, the Verdet constant is predicted to increase. This wavelength sensitivity provides a degree of freedom for identification of complex samples which contain more than one type of material; the spectrum of the Verdet constant can extract the constituents with methods employed in modern spectroscopy.

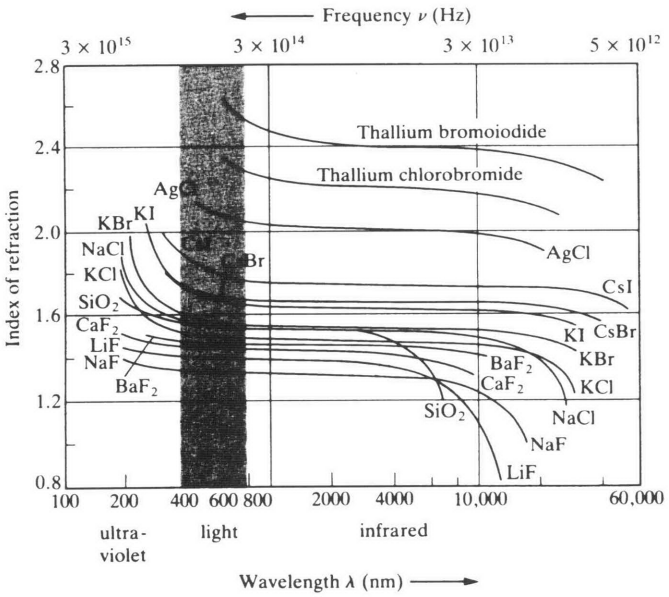

Figure 3-6: Plot of Indices of Refraction as a Function of Wavelength; from [11].

Material	Verdet Constant
Acetylene	330
Ethane	235
Benzene	3.00
o-Xylene	2.62
Glycerine	1.33
Ethyl Alcohol	1.131
Acetic Acid	1.044
Air	6.27e-6

Table 3.1: Verdet Constants at 589nm; minutes of arc/gauss-cm. Data from the CRC Handbook.

3.7 Modulated Faraday Rotation

Now that the physical basis for the Verdet constant has been explored, the practical considerations of implementing the Faraday effect as an optical modulation technique is discussed. The application of the Faraday effect to modulate the optical properties of a materials imposes one constraint on the modulation frequency. The general expression for the electrical wave equation,

$$-\nabla^2\vec{E} + \frac{1}{c^2}\frac{\partial^2\vec{E}}{\partial t^2} = -\frac{1}{c^2}\frac{\partial^2\chi\vec{E}}{\partial t^2},$$

must now include the partial derivative of the susceptibility tensor with respect to time. The complete equation including the time varying susceptibility tensor is

$$-\nabla^2\vec{E} + \frac{1}{c^2}\frac{\partial^2\vec{E}}{\partial t^2} = -\frac{1}{c^2}(\frac{\chi\partial^2\vec{E}}{\partial t^2} + \frac{\partial\chi\partial\vec{E}}{\partial t^2} + \frac{\vec{E}\partial^2\chi}{\partial t^2}).$$

Comparing the relative scales of the terms on the right half side,

$$\omega_m^2 \approx \omega_m\omega \approx \omega^2,$$

it is observed that for a modulation frequencies, ω_m, much slower than the electromagnetic wave frequency, ω, the wave dynamics simplify to the previous analysis. Practically, this constraint will always be obeyed with the modulated magnetic field, and the material being imaged will be in a state of quasi-equilibrium with respect to the Faraday effect.

3.8 Summary

The application of an external magnetic field to a homogeneous material transforms it into an optically active material. This phenomena is called the Faraday effect. The Faraday effect is found to be an excellent choice for modulating a material's optical properties for several reasons. As discussed in the previous chapter, the magnetic diffusion time constant insures good penetration of the modulating field into the sample. As found in this chapter, the relative timescales between the modulated field and electromagnetic wave propagating through the material insure that the susceptibility is always in a state of quasi-equilibrium. In addition, the differential nature of the Faraday effect helps to accentuate material differences with a large spread in Verdet constants. These theoretical observations are put into practive in the next chapter, which descibes the implementation of a Faraday effect imaging system.

Chapter 4

Implementation of the Modulated Faraday Effect Imager

4.1 Introduction

This chapter describes the implementation of a Faraday effect imaging system. The first section explores existing experimental techniques for observing the Faraday effect, their limitations, and how these limitations are solved by modulating the magnetic field. The remaining sections briefly describe the hardware, electronics, and software necessary to demonstrate the Faraday effect contrast technique. The use of "magic" sinewaves [17] are also explored as a method for improved synchronous demodulation.

4.2 Faraday Effect: Standard Measurement Techniques

This section briefly describes existing techniques for observing the Faraday effect and how they can be improved by modulating the external magnetic field.

4.2.1 Discrete Rotation of the Polarizer

A common approach to measuring the Faraday effect in a material is shown in Figure 4-1. The sample is placed in the field of an electromagnet. A monochromatic light source with a polarizer creates a polarized light beam that passes through the sample. After exiting the material, the

light passes through a second polarizer (analyzer) and strikes a photodetector. Initially no current flows in the magnet, and the second polarizer is rotated until light transmission is extinguished. This sets an initial reference state for the measurement of the Verdet constant. The coil is then excited with a current and a large magnetic field on the order of 1,000 gauss is applied to the sample. This field induces a rotation of the plane of polarization due to the Faraday effect, and the second polarizer is readjusted to extinguish the light striking the photodetector. By measuring the magnetic field strength, B_o, the length of the sample, l, and the rotation angle of the second polarizer, Φ, the Verdet constant for the sample is determined. This method is similar to that used by Faraday 150 years ago [4], and is used to demonstrate the effect in undergraduate Physics laboratories [20, 18]. Most existing techniques, including those used for thin-film magnetic structures, rely on the same general methodology [12, 3, 21, 6, 22, 1, 29].

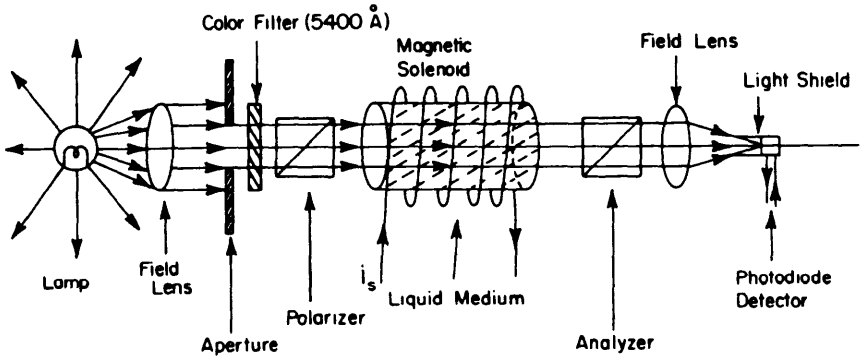

Figure 4-1: Common Experimental Design for Observing the Faraday Effect; from [18].

4.2.2 Limitations of Existing Methods

The existing methods for observing the Faraday effect are limited by two issues: insensitivity to small angular rotations and low-frequency noise. The extinction of light with a crossed polarizer is insensitive to small changes in the polarization angle. The instrument's sensitivity is defined as the incremental change in the transmitted light intensity (ΔI) for an incremental change in the angle of rotation ($\Delta\theta$). The angular dependence of polarizer sensitivity is found by analyzing the light transmission as a function of relative polarizer orientation, θ. The mathematical expression for the transmitted light intensity as a function of θ,

$$I = I_o cos^2(\theta),$$

is plotted in Figure 4-2. The incremental sensitivity of the crossed polarizers is found by taking the derivative of the intensity with respect to the angle θ,

$$S = \frac{\partial I_o}{\partial \theta} = 2I_o sin(\theta)cos(\theta),$$

and is plotted in Figure 4-3. The sensitivity is found to have zero magnitude when the polarizers are aligned at 0 degrees or crossed at 90 degrees, and have a maximum magnitude at 45 and 135 degrees.

The sensitivity of the crossed polarizers can be interpreted as the small-signal gain of a nonlinear amplifier. The intensity change of a polarizer pair to an incremental change in polarization angle is greatest at 45 and 135 degrees, and ideally the instrument should be biased into this region of highest gain. The problem with existing experimental approaches is that by *crossing* the polarizers to extinguish the light, the small-signal biasing is in a region of low gain. To circumvent this problem, some techniques take measurements at a number of polarizer angles and then extrapolate the angle of extinction[18].

A simpler scheme would be to cross the polarizers at an intermediate angle with higher sensitivity and look for small changes in the light intensity. This approach fails, however, because the intensity change from an applied magnetic field is imperceptible without substantial gain. For example, the change in transmitted intensity through 1 cm of water due to a 100

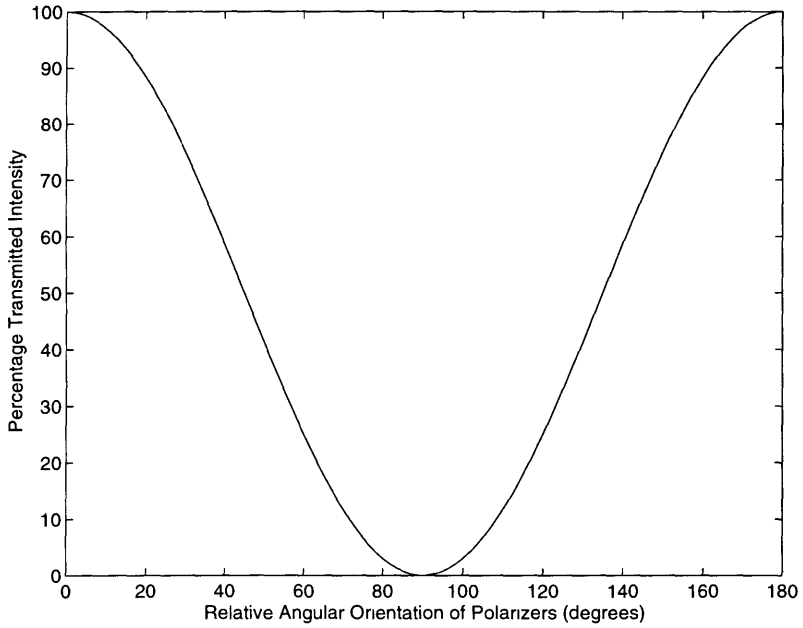

Figure 4-2: Transmission Intensity as a Function of θ.

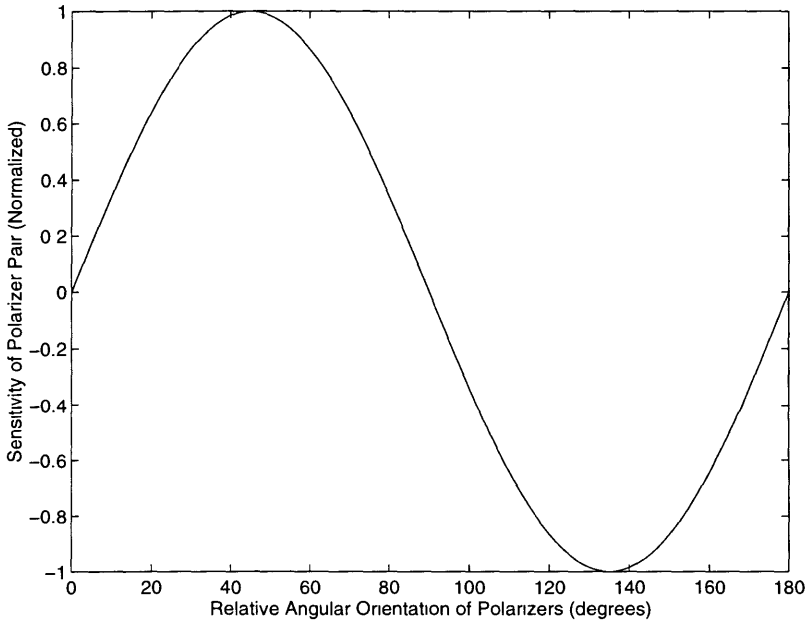

Figure 4-3: "Small-signal" Gain ($\frac{\delta I}{\delta \theta}$) for Crossed-Polarizers as a Function of θ.

gauss magnetic field is less than 1/1000 of the original signal. Passing the signal through a DC amplifier will not solve the problem for two reasons. First, the large optical background signal will generally saturate the amplifier long before the Faraday effect is resolved. Second, the noise in the measurement can dominate the signal at low frequencies.

Low frequency noise will limit the accuracy of a measurement if the signal from the detector is passed through a DC detector. This noise, generally referred to as drift or 1/F-noise, "can be introduced by long-term power fluctuations, changes in component values, temperature drifts, and other sources whose exact nature is poorly understood."[10]. The name 1/F arises from the fact that the spectral envelop of the drift noise varies roughly as 1/f, where f is the frequency in Hz[10, 13, 9]. Drift noise in the light source, detector, and electronics all act to limit the accuracy of the Faraday effect measurement. In experiments to date, the magnetic field was static during the measurements and susceptible to drift. If, however, the magnetic field is varied with time, the *modulated* Faraday effect signal could be pushed beyond the region of large 1/F noise. The full benefit of this approach is the subject of the next section.

4.2.3 Modulation of the Faraday Effect

Modulation of the magnetic field improves the accuracy of the Faraday effect measurement. By modulating the magnetic field the output of the photodetector may be synchronously detected. Synchronous detection allows for amplification of a specific frequency bandwidth, which if chosen correctly, lies in a region outside of 1/F dominated noise. This helps to improve the sensitivity of the measurement to small variations in the signal. The full benefits of synchronous detection will be covered in future sections, and are also covered extensively in the literature[10]. Another benefit of modulating the magnetic field is that the large background intensity of the light will be attenuated by the synchronous detector; this is similar to AC-coupling an oscilloscope to observe a small time-varying signal with a large DC offset. Still another advantage of this approach is that the polarizers may be biased at 45 degrees with respect to each other for maximum sensitivity to small angular displacements; the large amplitude of the illumination is no longer a problem. These benefits will theoretically improve the instrument's sensitivity to the Faraday effect. The remainder of this chapter provides an overview of the implementation of these ideas in an imaging system.

4.3 Instrumentation Overview

This section describes the implementation of the Faraday effect imaging system. The section is broken down broadly into a hardware overview, electronics overview, a discussion of signal processing issues, and a description of the data acquisition system.

The imaging system is briefly outlined here; refer to Figure 4-4. A laser creates a collimated light source which passes through a polarizer. This sets the initial polarization state of the light. The light beam then passes through an electromagnet with the sample placed in the middle. The field of the electromagnet is modulated externally by an H-bridge power supply. After the light passes through the material and exits the electromagnet, a second polarizer crossed at 45 degrees converts its polarization state into an intensity signal. The intensity is measured by a photodetector whose is output synchronously detected. Both the synchronous detector and the H-bridge power supply are controlled by a microcontroller to insure they are synchronized. Finally, a two-axis scanner moves the sample through the gap of the electromagnet while the

data acquisition system records the Faraday effect signal at selected points in the sample.

4.3.1 Hardware Overview

Magnet

The electromagnet used in this instrument was a Leybold 562-32, which is illustrated in Figure 4-5. The core of the magnet has an .125" hole bored through the core to facilitate axial optical measurements. A sample is then placed in the gap between the magnet poles.

The synchronous detection of the Faraday effect requires that the magnetic field be linearly related to the current in the coil. In electromagnets, this can be a problem due to saturation of the electromagnet's core permeability[14]. The magnetic field in the gap is approximately

$$B = \frac{Ni\mu_o}{g(1 + A_g/A_c(\frac{\mu_o l}{\mu_c g}))},$$

where N is the number of turns (500), μ_o is the permeability of free space, μ_c is the permeability of the core, g is the gap width, i is the current, and A_g and A_c are the area of the gap and core, respectively. By constraining the gap width,

$$g \gg \frac{A_g \mu_o l}{A_c \mu_c},$$

the magnetic flux is made independent of the material's permeability. The expression for the magnetic field then reduces to

$$B \approx \frac{Ni\mu_o}{g}.$$

The physical dimensions of the magnet and the high permeability ($\mu_c \gg \mu_o$) insure that this inequality is met.

The magnet has a rated inductance of 4.4mH and a series resistance of 1.2Ω. These electrical terminal characteristics permit modulation of the coil current on the order of tens of Hertz with modest power circuitry. Using the expression found previously, magnetic fields on the order of 1000 gauss require 1.6A of current through the coils.

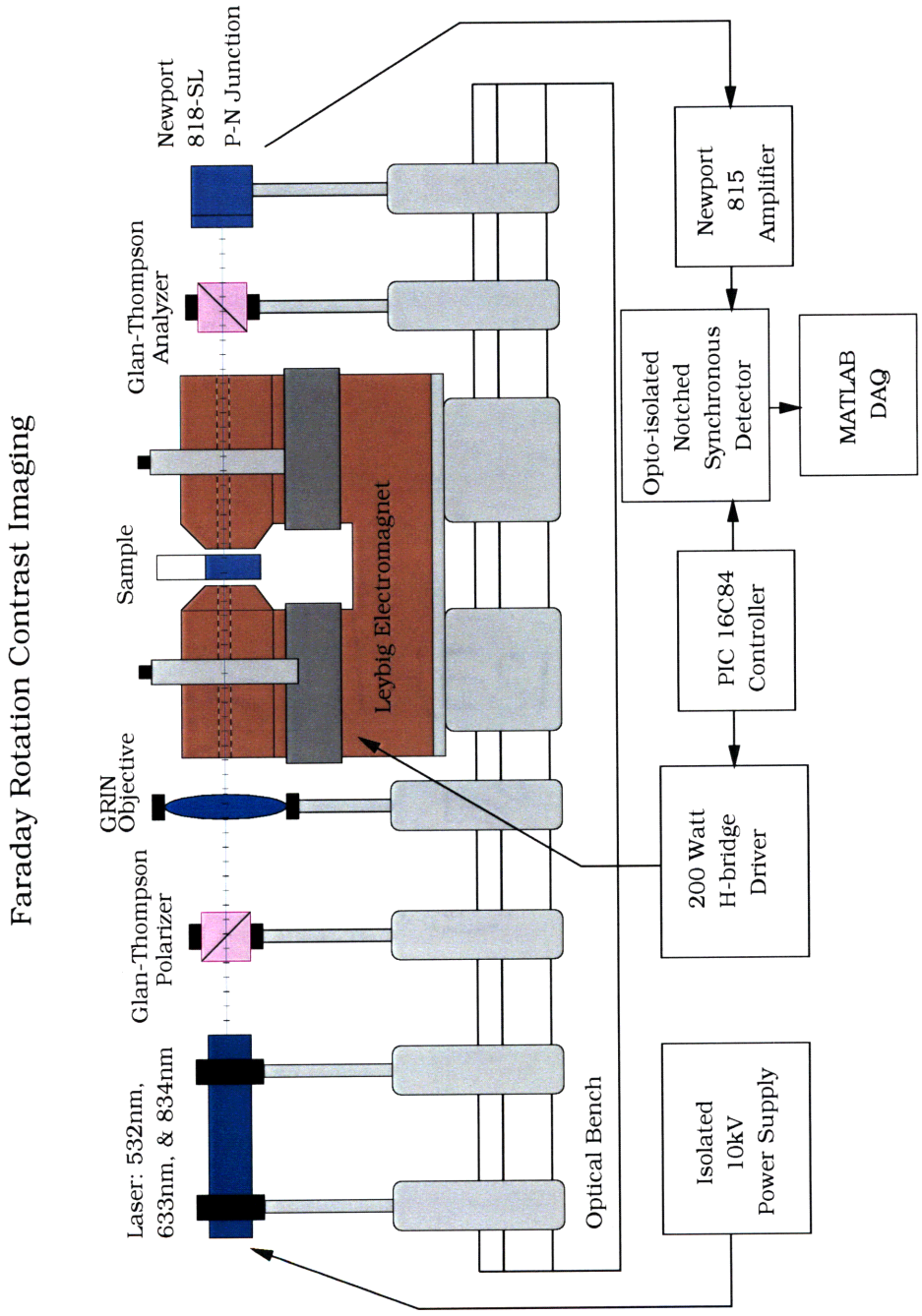

Figure 4-4: System Design for Scanning Rotation Imager.

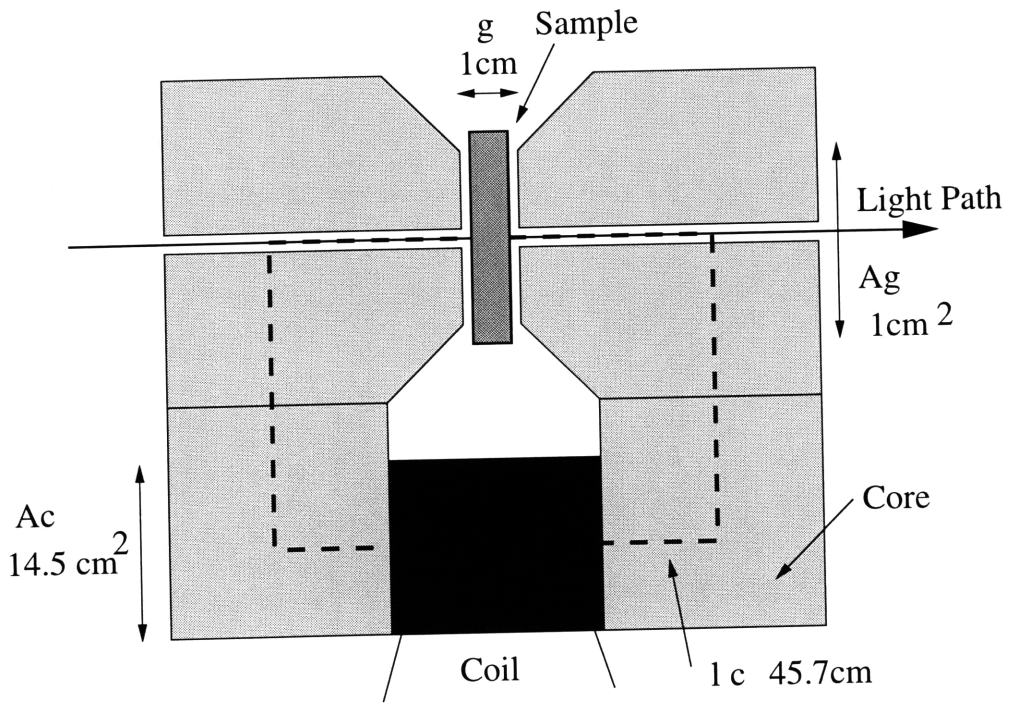

Figure 4-5: Geometry the Leybold Electromagnet; Not to Scale.

Laser

A laser was chosen as the light source because of its illumination intensity and beam collimation. The power output of a laser can generally be resolved by a Newport 815 optical power meter[1], and the collimation of the laser beam eliminated the need for focusing optics in the prototype, which is designed for resolution of approximately 1mm.

Three lasers were explored as possible light sources. The initial experiments were performed with a 5mW, 625.5nm helium-neon (He-Ne) gas laser from SpectraPhysics. The power module for this laser uses the 110V utility service. When the electromagnet is being modulated, the fluctuations of the service feed into the laser output. This feedthrough creates a signal that has no relation to the Faraday effect, and its magnitude swamps the actual signal of interest. To fix this problem, a solid-state laser diode powered by a battery is used. The battery supply effectively isolates the light source from the magnet drive, and the 635nm, 5mW laser diode from Meredith Instruments has essentially the same optical characteristics as the original He-Ne laser. The laser diode is powered by a current source with optical feedback provided by a second diode mounted parallel to the laser. This feedback improves the disturbance rejection from temperature drift and battery voltage fluctuations.

A third laser source was constructed to explore the wavelength dependence of the Verdet constant. A He-Ne laser was modified by Meredith Instruments to provide radiation at 532nm. The output power of this laser was only 0.2mW, however, and could not be resolved by the Newport optical power meter.

Photodetector

The light intensity was measured by a Newport 818-SL photodetector. The output current from the photodetector was amplified and displayed by a Newport 815 optical power meter. The Newport 815 also has a transresistance amplifier with a bandwidth of 10kHz. This bandwidth is well above the modulation frequency of the magnetic field ($\approx$ 10Hz), and the variations in signal intensity due to the Faraday effect are easily resolved.

[1]This was the instrument available from the Modern Optics Project Laboratory at MIT.

Polarizers

Glan-Thomson polarizers were used as the polarization devices. The Glan-Thomson device has an extinction ratio, defined as the magnitude of light transmitted when a polarizer pair is aligned to the magnitude when crossed, of $10^5 : 1$. Polaroid film, on the other hand, has an extinction ratio of only 100:1. The polarizers were mounted in a rotating assembly labeled with a protractor that allowed for accurate manipulation of the angle between the polarizers.

4.3.2 Electronics Overview

Magnet Current Source

The electromagnet's coil is driven by an H-bridge topology shown in Appendix A. The four bridge transistors are IRF530N nfets from International Rectifier. The FETs are controlled by an LT1162CN gate driver chip. The LT1162CN has an opto-isolated drive circuit that provides the necessary turn-on voltage for the top two FETs in the bridge. Control of the LT1162CN requires four inputs, each corresponding to one FET. A digital logic circuit was constructed that supplies the necessary gate control with a two-bit sequence. One bit controls the side of the bridge connected to ground, and thereby the voltage polarity across the load. The second bit controls the actual voltgae applied by toggling between V_{dd} and ground. Using this two-bit control scheme allows for the implementation of complex voltage drive sequences. The advantages of these drive sequences will be discussed in the section on signal processing issues.

Synchronous Detector

The basic system diagram for synchronous demodulation is given in Figure 4-6. The signal of interest is generally modulated at a frequency above the 1/F noise prior to entering the detector; this instrument modulates the intensity by the varying magnetic field. Upon entering the demodulator, the signal is selectively amplified by a bandpass amplifier centered at the modulation frequency. To sample the signal after amplification, it is multiplied by a demodulation waveform at the same frequency. The multiplication reflects the original signal at ω_m to DC and $2\omega_m$ (with half the amplitude), and the DC value is sampled after low-pass filtering. The waveform used for demodulation has interesting repercussions on the performance of the

demodulator.

One method of multiplication uses a sinusoidal waveform and analog multiplier. Analog multipliers, however, suffer from signal-to-noise problems due to their restricted region of linearity. The use of linear multiplication constrains the signal size to the order of kT/q, where thermal noise can be significant and the benefits of synchronous detection are diminished[23]. In addition, it is difficult to create a pure sinusoid at arbitrary frequency. A simpler approach is to multiply by a square wave. This technique can be implemented with the multiplication block shown in Figure 4-7. By toggling the switch SW1 with a 50% duty ratio, the signal input is multiplied by a square wave of amplitude 1. The issue with squarewave demodulation is that higher order harmonics fold noise back into the signal path. This problem will be revisited in the section on signal processing issues.

A synchronous detector was constructed using square-wave demodulation. The bandpass preamplifier was constructed using a bridged-T filter in the feedback path of an LT1007 operational amplifier. The bridged-T circuit creates a notch filter at frequency $\omega = (RC)^{-1}$, with an attenuation factor of $(1 + C_1/2C_2)^{-1}$. When used as a feedback element, the notch circuit results in a bandpass amplifier with gain $(1 + C_1/2C_2)$ at a frequency of $(RC)^{-1}$. The actual elements used for this implementation created a gain of 200 at a frequency of 12Hz; a frequency well above the 1/F noise for the imaging system[2]. The numbers were verified in a MATLAB simulation of the notch circuit shown in Figure 4-9.

The multiplier element of the circuit is shown schematically in Appendix A and figuratively in Figure 4-8. The input of the circuit is buffered with a low-noise LT1007 opamp. The multiplication element uses a high speed LT1191 opamp with a LTC1043CN chip that serves as the switching element. The switch controls for the LTC1043CN are derived from a PIC16C84 microcontroller. The PIC 16C84 also drives the input logic for the magnet coil drive, insuring the two circuits are synchronized[3]. The output of the multiplier subcircuit is buffered by a second LT1007 low-noise opamp acting as a low-pass filter. An additional LT1043CN switch was added to the basic multiplication block. This switch, SW2, allows the signal to the output buffer to toggle between the multiplier output and ground, similar to the second control bit on

[2]The 1/F noise was measured with a Hewlett-Packard Spectrum Analyzer.

[3]The ninety degree phase shift between applied voltage and resulting current in the electromagnet was accounted for in software

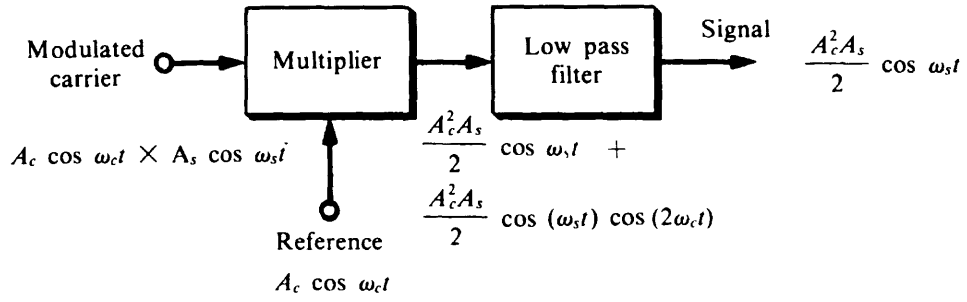

Figure 4-6: System Diagram for a Synchronous Demodulator; from [10].

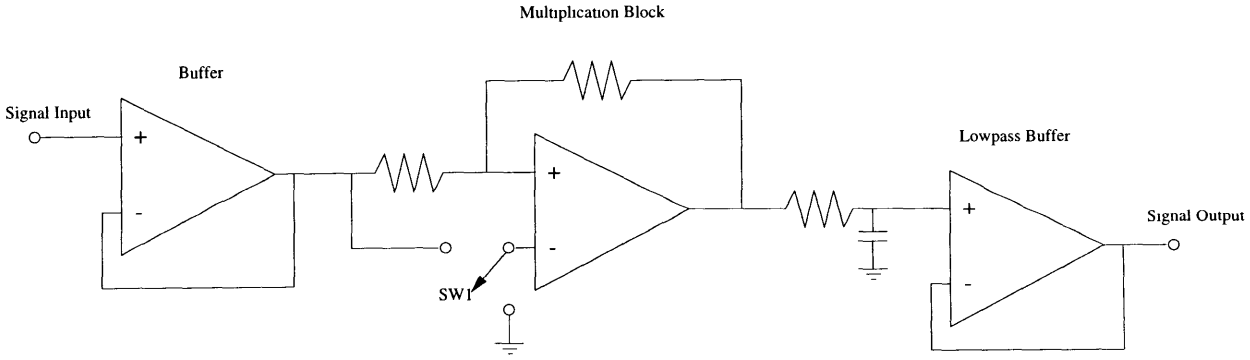

Figure 4-7: Standard Implementation of Synchronous Demodulator.

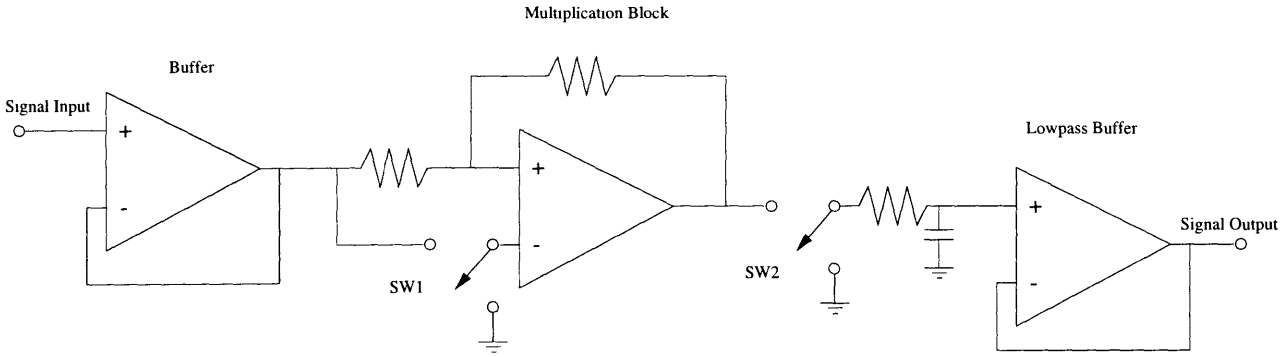

Figure 4-8: Modified Synchronous Demodulator. SW2 Allows for Implementation of the Magic Sinewave Bit Sequence.

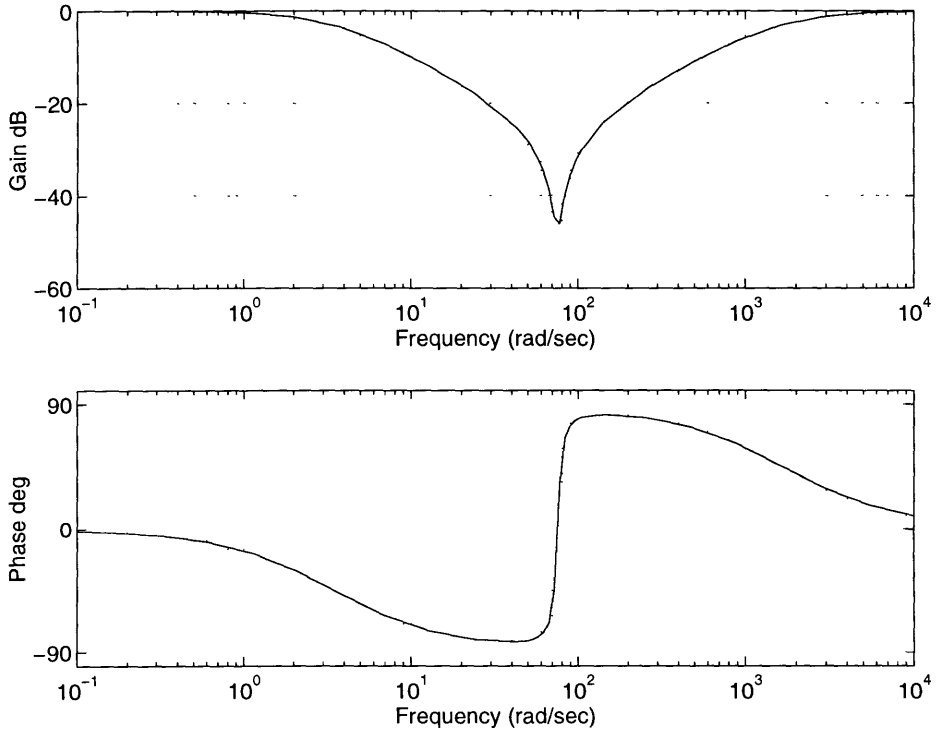

Figure 4-9: Bode Plot of Bridge-T Circuit.

the bridge control. The advantages of this extra switch are discussed in the next section.

4.3.3 Signal Processing Issues

Textbook synchronous detection schemes generally modulate the signal of interest as a sinusoid and demodulate by linear multiplication with a second sinusoid. Practically, however, both the modulation and demodulation steps are implemented with binary switching circuits. For the modulation of the magnetic field, a switching circuit is required due to the current magnitude and switching period; a linear implementation of this circuit would require expensive components and waste considerable power. The synchronous detector uses binary switching for two reasons: first, it is simple to implement, and second, linear multipliers suffer from noise issues discussed previously. Lancaster, however, has described a binary switching pattern, called a magic sinewave, that emulates sinusoidal waveforms[17]. By driving the electromagnet and synchronous detector with magic sinewaves, the "textbook" synchronous detection scheme can essentially be implemented.

Analysis of Magic Sinewaves

The use of complex bit patterns, defined as magic sinewaves [17], allows a circuit to emulate a sinusoidal waveform with binary switching. The underlying concept of the magic sinewave is similar to the notching technique in power electronics. By selectively removing, or "notching", a waveform appropriately, arbitrary harmonics can be removed. Figure 4-10 illustrates this technique for removing the third and fifth harmonics from a square wave. If the system of interest has a lowpass property, the higher harmonics will be attenuated and the resulting waveform will then to first order be a sinusoid. The magic sinewaves take the concept of notching a step further. The magic sinewave splits up the period of a waveform into a predetermined number of m bits, which may be either "on" or "off". Analysis of the bitstream's harmonic content dictates what the state of each bit should be given the constraints on the harmonic content for the waveform.

The magic sinewave is analyzed as a superposition of m identical square waves shifted in time, see Figure 4-11. In the frequency domain, the harmonic content is a superposition of sinc

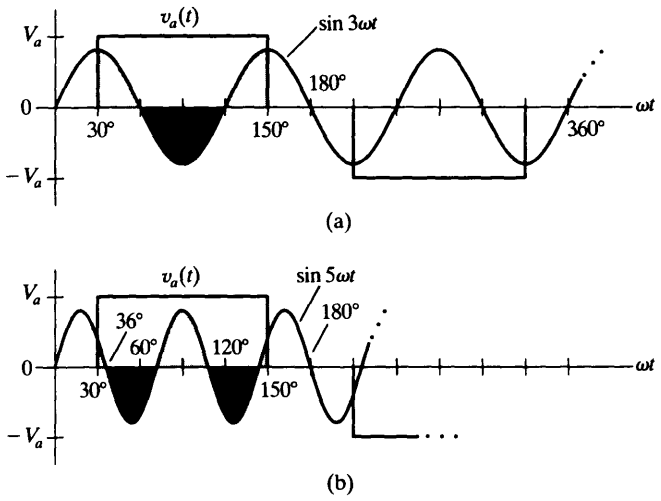

Figure 4-10: Notching a Squarewave to Remove Harmonics; from [14].

waveforms,

$$\mathcal{F}(f) = exp(-\pi jfT) \sum_{k=0}^{m} A(k) exp(-2\pi jfTk) \frac{sin(T\pi f)}{\pi f},$$

multiplied by a phase resulting from their relative time offsets. The factor $A(k)$ is a binary operator that determines if the bit k is "on" or "off". The bitstream is periodic with time, $\tau = mT$, where T is the period of one bit in the magic sinewave. The harmonic content is therefore multiplied by a series of delta functions,

$$\mathcal{F}(f) = exp(-\pi jfT) \sum_{k=0}^{m} A(k) exp(-2\pi jfTk) \frac{sin(T\pi f)}{\pi f} \sum_{n} \delta(f - n/\tau).$$

Both the sinc and phase term $exp(-\pi jfT)$ are common to all terms, and removed from further consideration. Using the relationship between τ and T, the analysis of the magic sinewaves reduces to a sum of phase offsets,

$$\mathcal{F}'(f) = \sum_{n} \sum_{k=0}^{m} A(k) exp(2\pi jnk/m),$$

where n is a harmonic frequency and k is a bit in the magic sinewave. To remove a particular harmonic n, the $A(k)$ are chosen such that the sum of the phases for bits with $A(k) = 1$ add to zero.

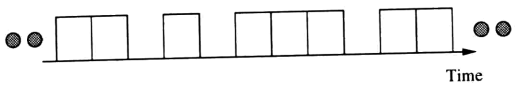

Figure 4-11: Magic Sinewaves are easily analyzed as a bitstream.

Two further assumptions help to simplify analysis. First, if the bitstream for one half-period is anti-symmetric with respect to the other half-period, then all even harmonics are equal to zero. Second, if the bitstream is symmetric within each half-cycle, then the phase summation reduces to analyzing the complex component of the phase for the first quarter-cycle of the magic sinewave:

$$\mathcal{F}'(f) = \sum_{n}\sum_{k} A(k)exp(2\pi jnk/m) \rightarrow \sum_{n,odd}\sum_{k=0}^{m/4} A(k)sin(2\pi jnk/m).$$

These symmetry assumptions are illustrated in Figure 4-12. The problem is now reduced to selecting the optimal array of $A(k)$ factors to suppress higher order harmonics of concern.

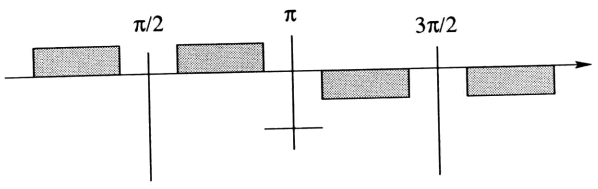

Figure 4-12: Symmetry assumptions for the bitstream.

The analysis of the phase summations is compactly solved using matrix multiplication. The

first matrix,

$$\begin{pmatrix} 0 & 0 & 0 & \cdots \\ 0 & 0 & 1 & \cdots \\ 0 & 1 & 1 & \cdots \\ \vdots & \vdots & \vdots & \vdots \end{pmatrix}$$

represents the possible bitstreams; each row is one possible magic sinewave. The second matrix represents the phase content from each bit k in the magic sinewave,

$$\begin{pmatrix} sin(0) & sin(0) & sin(0) & \cdots \\ sin(1\Phi) & sin(3\Phi) & sin(5\Phi) & \cdots \\ sin(2\Phi) & sin(6\Phi) & sin(10\Phi) & \cdots \\ \vdots & \vdots & \vdots & \vdots \end{pmatrix}.$$

where $\Phi = 2\pi/m$. Each row in this matrix represents a single bit's phase offset for a series of harmonics; each column represents the phase shift for each bit in the magic sinewave for a particular harmonic. Note that the total number of columns in the phase matrix is arbitrary, and determined by the number of harmonics of interest.

Multiplication of these two matrices gives the net phase coefficient for each possible bit pattern at the harmonic frequencies of interest. Each column in the resulting matrix identifies the net phase summation for a particular harmonic; the rows correspond to the harmonic series for a specific bit pattern. To choose a magic sinewave, a row is chosen from the matrix that has zeros in the appropriate columns (harmonics) of interest. This analysis tool has given produced magic sinewave patterns of up to 210-bit resolution with relative computational efficiency. A sample 210-bit waveform[17] is illustrated in Figure 4-13, and the harmonic content is given in Table 4.1. For very large bitstreams, this technique is computationally intensive. Alternative search algorithms for larger magic sinewaves are then available, although they do not guarantee the optimal solution[25].

Application of Magic Sinewaves: Driving the Electromagnet

Figure 4-14 illustrates a 30-bit magic sinwave used to drive the Leybold electromagnet. The two digital traces are the control bits for the bridge driver discussed previously; the top digital

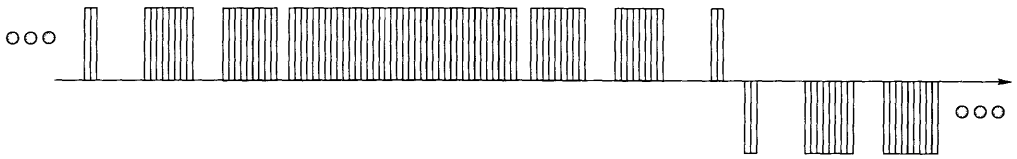

Figure 4-13: Bit pattern for a 210-bit Magic Sinewave.

Harmonic Number	Harmonic Content
Fundamental	0dB
2nd	-60dB
3rd	-60dB
4th	-65dB
5th	-58dB
7th	-60dB
9th	-62dB
11th	-53dB
13th	-30dB
15th	-40dB
17th	-13dB
19th	-15dB

Table 4.1: Harmonic Elimination for a 210-bit Magic Sinewave.

trace toggles the arm of the bridge, the bottom trace toggles the other arm between positive voltage and ground. The first significant harmonic for a 30-bit sinewave is the eleventh[17], which is well above the -3dB point for the electromagnet. The higher harmonics are therefore attenuated and the resulting current waveform is a relatively pure sinusoid at the fundamental frequency of 12Hz.

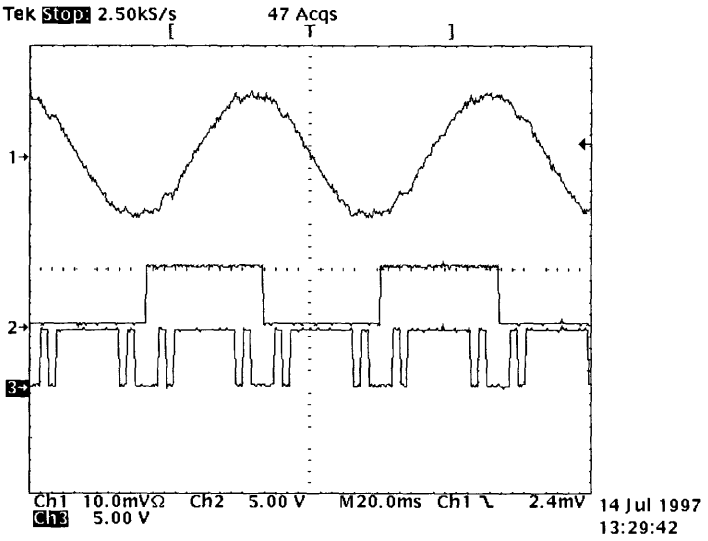

Figure 4-14: Demonstration of Sinusoidal Current Drive through Electromagnet; Driven with 30-bit Magic Sinewave.

Application of Magic Sinewaves: Synchronous Demodulation

A major disadvantage of using square wave demodulation in a sychronous detector is that the frequency content of the square wave is quite rich; the odd-harmonics fall off at a modest 20dB/decade. If the sinusoidal signal being detected is at the fundamental of the square wave, then the frequency content of the square wave at higher harmonics will result in excess noise being reflected back into the measurement.

This is understood by revisiting the multiplication of the demodulation and signal wave-

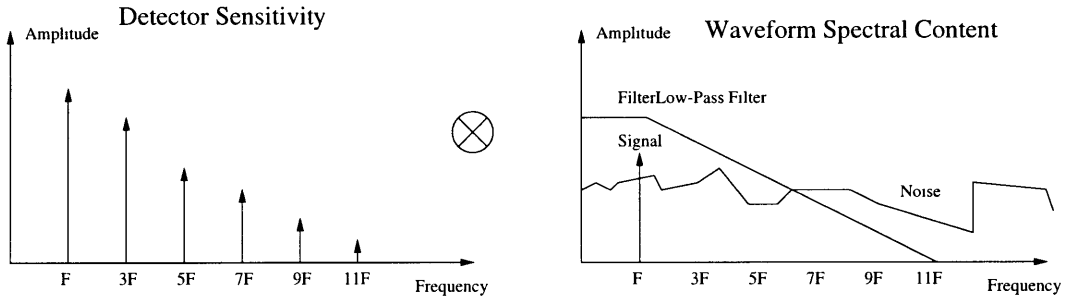

Figure 4-15: Convolution of Input Signal with Squarewave Demodulation Waveform. The detector sensitivity represents the harmonic content of the demodulation waveform, and the waveform spectral content represents the harmonic content of the signal input.

forms. The multiplication of the signal and demodulation waveform in time represents a convolution in the frequency-domain. The instantaneous DC output of the multiplication will therefore be the projection of the square wave harmonic content onto the spectral profile of the signal and noise, as Figures 4-15 and 4-16 illustrate. The instantaneous detector output will be

$$V_{out} = \int V_{signal}(f) \cdot \Lambda(f) df + \int V_{noise}(f) \cdot \Lambda(f) df,$$

where $\Lambda(f)$ is the detector sensitivity as a function of frequency, and is simply the harmonic content of the demodulation waveform. Using the fact that the detector sensitivity is a sum of shifted delta functions due to its periodicity in time, the instantaneous DC output of the demodulator reduces to

$$V_{out} = V_{signal}\Lambda(f_o) + \sum_{f=f_o}^{n} V_{noise}\Lambda(f).$$

Ideally, the noise summation would only include the fundamental term, f_o, but the harmonic content of the square wave can allow for substantial noise sensitivity. Removal of the noise through input filtering is difficult, since the detector is sensitive to noise only a factor of three above the demodulation frequency. To help address this problem, the output voltage is low-pass filtered. The lowpass filter not only eliminates the signal component at $2\omega_m$, but also helps to

reduce the noise component through averaging. The use of lowpass filtering, however, creates a trade-off between the signal-to-noise ratio and detector bandwidth.

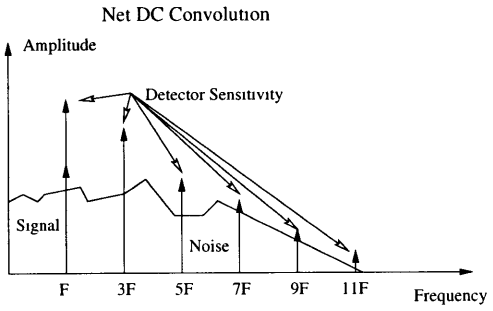

Figure 4-16: Net DC Convolution of Noise/ Input Signal with Magic Sinewave. The instantaneous DC output of the multiplier is the net projection of the demodulation waveform and the waveform spectral content.

The use of a magic sinewave can improve the noise performance and/or bandwidth of the synchronous detector. As shown in section 4.2.1, the use of a magic sinewave pushes the unwanted harmonic content out to higher frequencies. The detector's sensitivity at lower harmonics is then removed, and the increased sensitivity at higher frequencies is of lesser concern due to the ease of implementing an input filter. If the bitstream pattern and input filter are chosen appropriately, it is possible to approach the ideal instantaneous detector output

$$V_{out} = V_{signal}\Lambda(f_o) + V_{noise}(f_o)\Lambda(f_o).$$

The implementation of this scheme requires only an additional switch and control bit from the PIC16C84.

The spectral sensitivity of the synchronous detector was measured as a function of frequency using a Hewlett-Packard spectrum analyzer. These measurements were taken both in standard square-wave mode, and by notching with a 210-bit magic sinewave. The data is presented in Table 4.3.3. The sensitivity to harmonic noise is essentially eliminated until the 17th harmonic. To illustrate the principle of the notched detector in the time domain, a series of plots were

captured with the Tektronix 420 oscilloscope, and are included in Appendix C. The fundamental and first two odd harmonics show a net DC amplitude when chopped with a square wave. With a suitably notched waveform (210-bit in this case), however, the fundamental can maintain a finite DC component, while the third and fifth harmonic average to zero.

Harmonic	Standard Synch Theory	Standard Synch Data	Magic Synch
Fundamental	0dB	0dB	0dB
2nd	-	-65dB	-60dB
3rd	-9.5dB	-8dB	-60dB
4th	-	-70dB	-65dB
5th	-14.0dB	-14dB	-58dB
7th	-16.9dB	-18dB	-60dB
9th	-19.1dB	-20dB	-62dB
11th	-21.8dB	-20dB	-53dB
13th	-22.3dB	-20dB	-30dB
15th	-23.5dB	-24dB	-40dB
17th	-24.6dB	-25dB	-13dB
19th	-25.6dB	-26dB	-15dB

Table 4.2: Comparative results of synchronous detection. Data illustrates excellent low harmonic cancellation with notching, and relative gain of 17th and 19th harmonics. Note: Data taken with 250Hz fundamental.

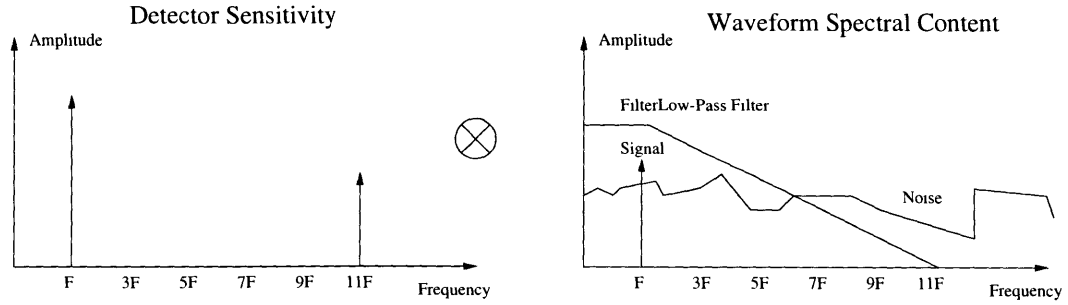

Figure 4-17: Convolution of Input Signal with Magic Sinewave. The detector sensitivity is the harmonic content of the magic sinewave, and the waveform spectral content represents the harmonic content of the signal input.

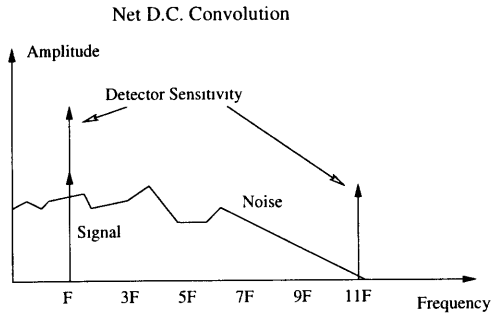

Figure 4-18: Net DC Convolution of Noise/ Input Signal with Magic Sinewave. The instantaneous DC output of the multiplier is the net projection of the demodulation waveform and the waveform spectral content.

4.3.4 Data Acquisition and Scanning Control

Data Acquisition

The data acquisition system used a Genie card from Advantech. The Genie card is a general purpose interface board, with digital I/O, digital-to-analog (D/A), and analog-to-digital (A/D) functionality. A driver was written for the board using cmex functions in MATLAB; the code is provided in Appendix B. Briefly, Adcconfig.c configured the A/D controller for gain, scan range, and trigger source, Cntconfig.c sets the clock rate for triggering the A/D, and Fetch2.c reads in an array of datapoints, the size of the array determined the user.

Scanner and Control

A scanning stage was created from the two-axis scanner shown in Figure 4-19. Airpax model 4SH-6AS stepper motors served to adjust the position of the sample. To control the movement of the motors, two cmex functions, goleft.c and goright.c, were linked to MATLAB. These functions supply the control bits to the stepper motor driver boards, whose schematic is provided in Appendix A. Combining these scanner functions with the previous acquisition software, it is a simple matter to design an experiment by creating a MATLAB *.m function. An example for a two-dimensional scanning sequence, "scan2d" is given in Appendix B.

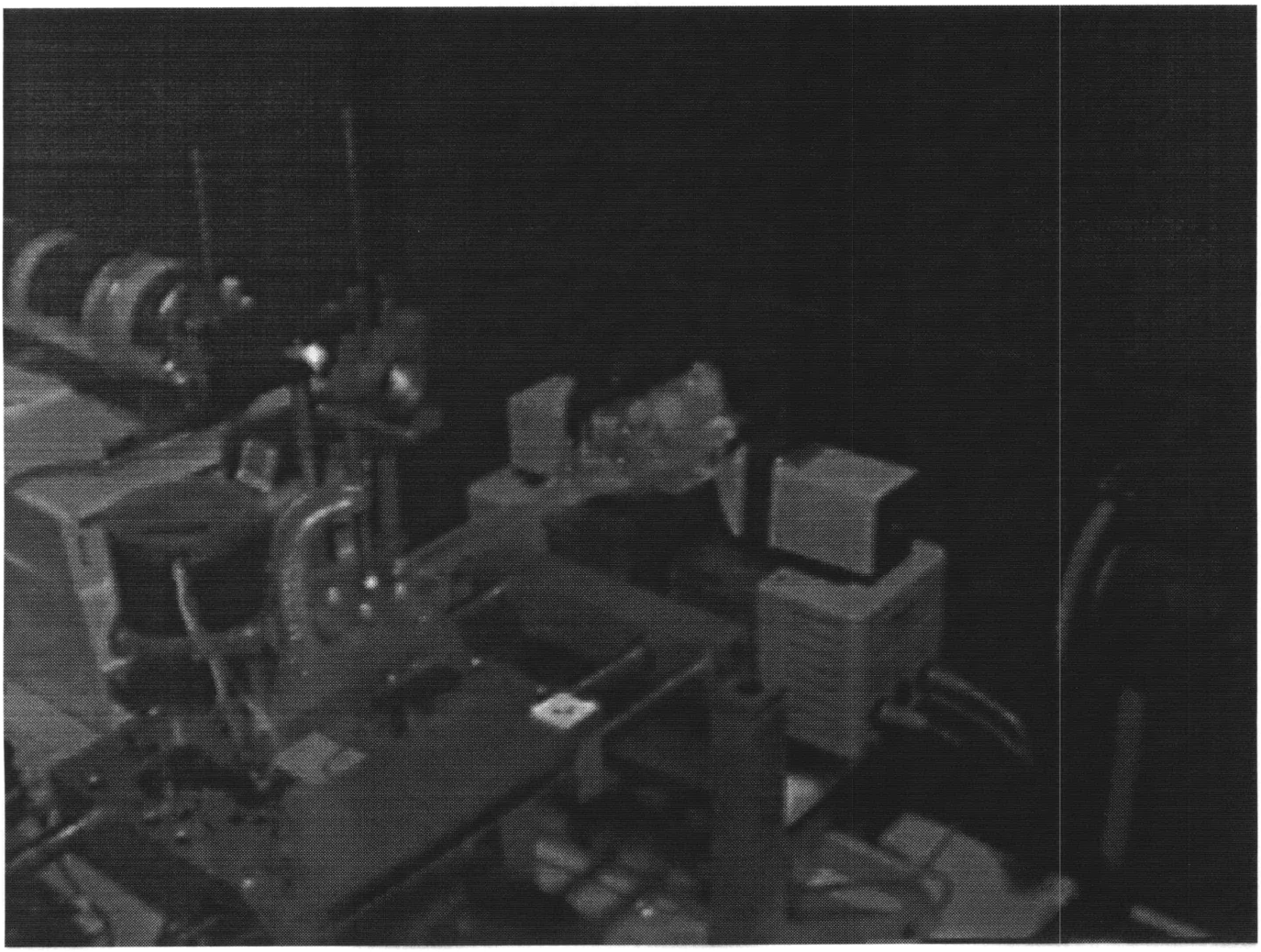

Figure 4-19: Photograph of the Two-axis Scanner.

4.4 Summary

This chapter described the implementation of an imaging system based on modulation of the Faraday effect; a picture of the complete scanning system is shown in Figure 4-20. A complete optical system for analyzing the polarization properties of light was constructed. An electromagnet was AC modulated so that the Faraday effect properties of a material could be synchronously detected. The use of magic sinewaves to drive both the electromagnet and synchronous detector allowed for increased noise immunity for little extra circuitry. The interface of MATLAB to the scanner controls and synchronous detector output results in an autonomous scanning system. The preliminary results of this imager are the described in the next chapter.

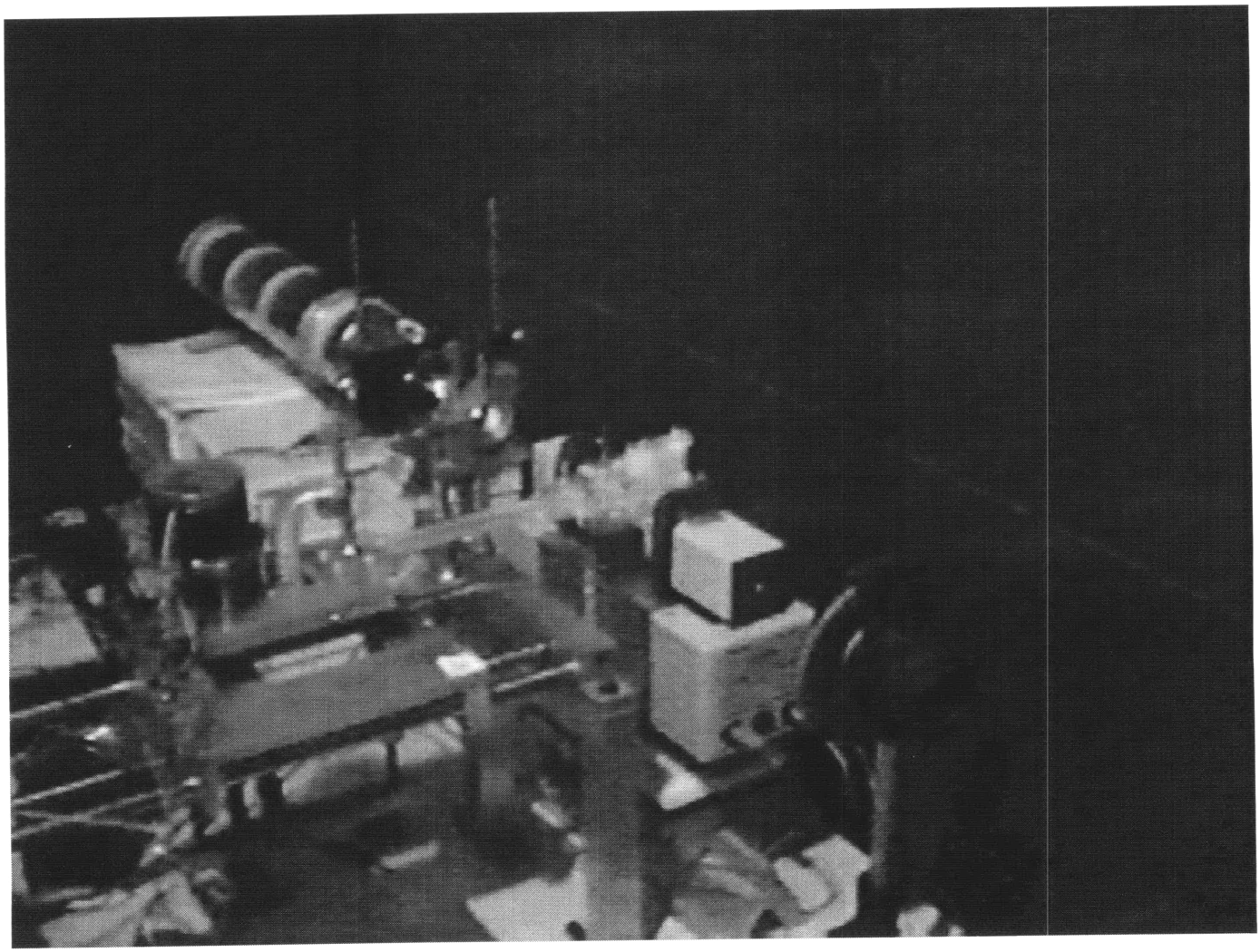

Figure 4-20: Photograph of Faraday Effect Imager.

Chapter 5

Results of Faraday Effect Imaging System

5.1 Introduction

This chapter briefly discusses the results of the Faraday Effect imager developed in Chapter 4. Its purpose is to give a short overview of the types of measurements available with the Faraday Effect imager. The first section verifies the small-signal characteristics of the crossed polarizer system. The measurement of Verdet constants is then described and compared with data in the literature. The imaging capabilities of the instrument are then explored, and future directions discussed.

5.2 Small-Signal Sensitivity of Crossed Polarizers

This section explores the verification of the "small-signal" properties of a polarizer pair introduced in Chapter 4. The small-signal sensitivity for a polarizer pair was defined as the change in the transmitted intensity for an incremental change in the polarization angle, θ. The mathematical expression for this sensitivity,

$$S = 2I_o sin(\theta)cos(\theta),$$

is plotted in Figure 5-1.

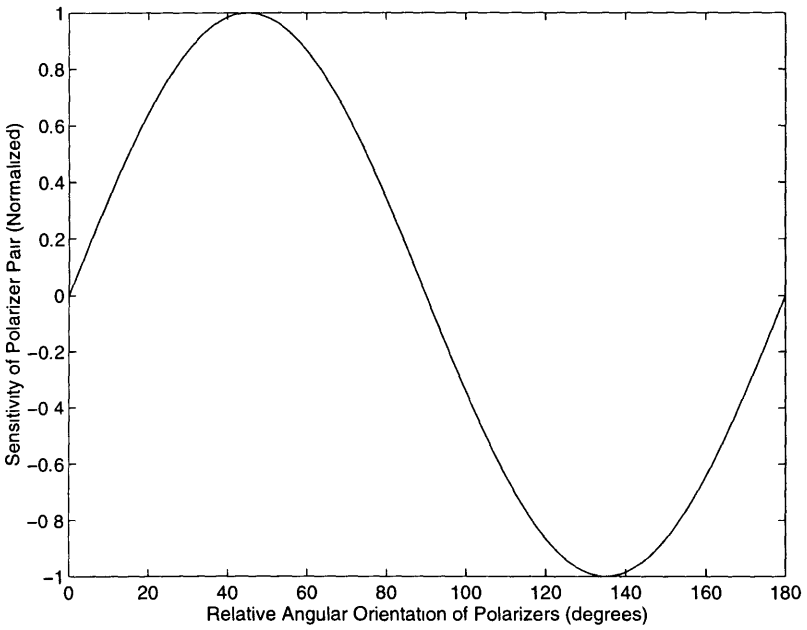

Figure 5-1: "Small-signal" Gain ($\frac{\delta I}{\delta \theta}$) for Crossed-Polarizers as a Function of θ.

To verify small-signal characteristics of the polarizer pair, a series of datapoints was collected for a number of angular positions, θ. The output of the photodetector was then synchronously detected with reference to the modulated magnetic field. The data is plotted in Figure 5.2.

The excellent correlation between theory and experiment verifies the small-signal characteristics of a crossed polarizer pair. In addition, it confirms the sensitivity of the instrument to *time-varying* changes in light intensity and not absolute intensity.

5.3 Measuring the Verdet Constant

This section discusses an experiment to measure the *relative* Verdet constants of transparent fluids. Three solutions were prepared that are commonly used in undergraduate physics labs: carbon disulfide (CS_2), distilled water (H_20), and o-Xylenes. Each solution was placed into the Faraday Effect imager and the output voltage recorded for a series of current magnitudes. The

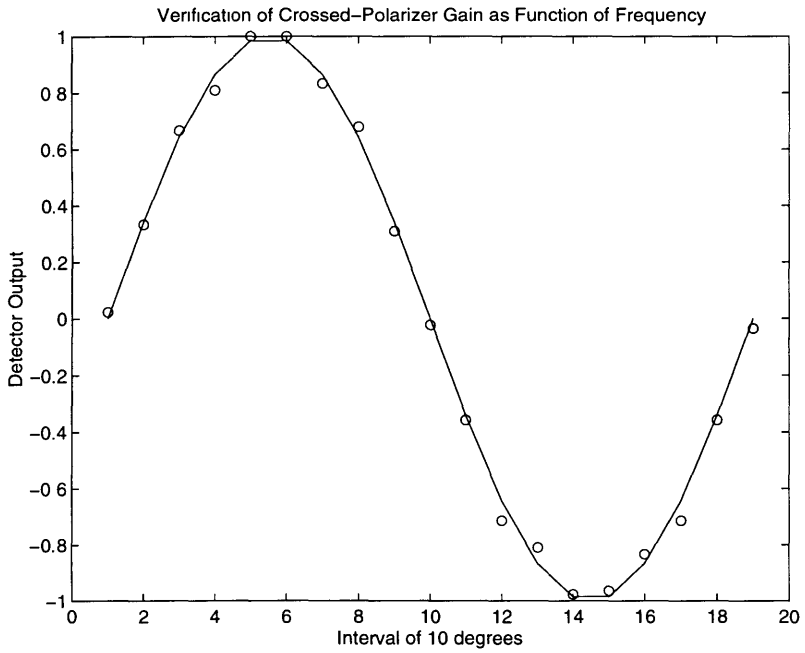

Figure 5-2: Comparison of Theoretical Detector Output with the Measured Signal. Note that the first datapoint corresponds to the polarizers being aligned.

data is shown in Figure 5-3.

To determine the relative Verdet constants, the slopes for each line are compared. The results of this experiment are presented with data from [18] in Table 5.3. The advantage of the modulated magnetic field is now evident. Loeffler's method required measurements at several angles and curve-fitting to obtain reasonable data[18]. The data collected with the modulated Faraday effect in Figure 5-3 demonstrates the excellent signal-to-noise ratio for the instrument, which allows for data collection with *one* measurement.

Material Ratio	Faraday Effect Imager	Literature (Loeffler)
CS_2 : H_20	3.16	3.00
o-Xylenes : H_20	2.20	1.99

Table 5.1: Comparison of Relative Verdet Constants.

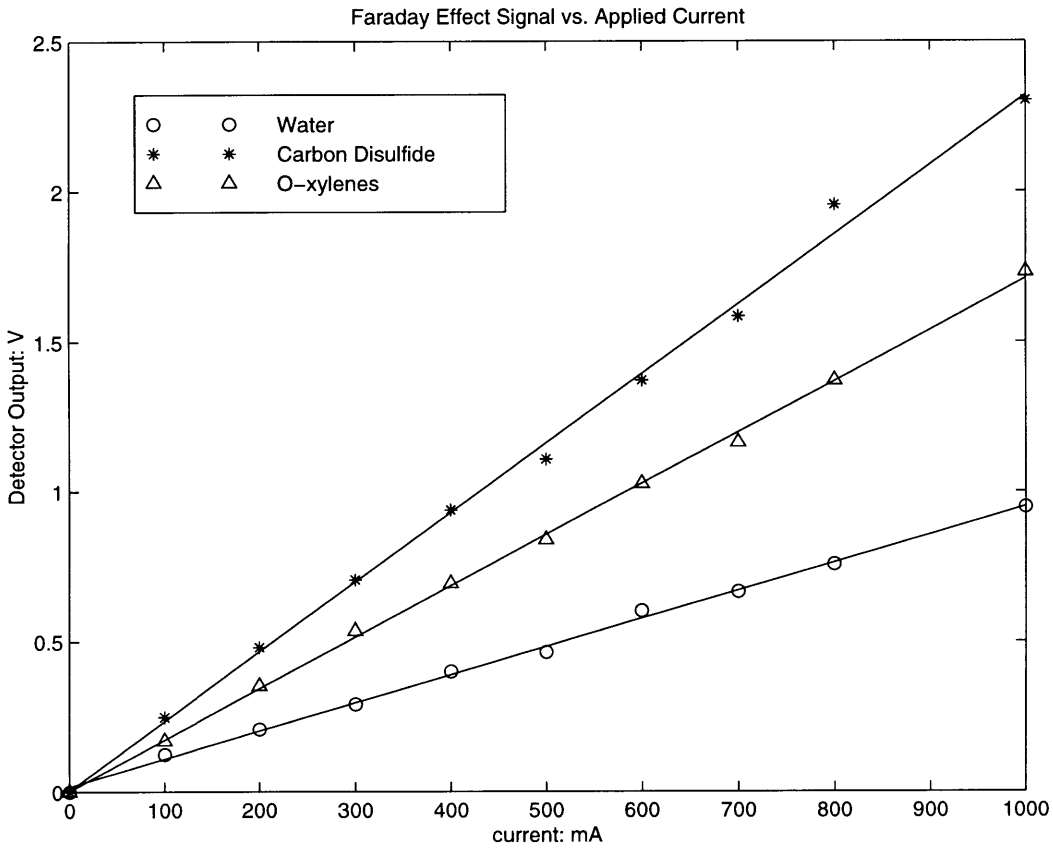

Figure 5-3: The Measurement of the Relative Verdet Constants. Relative Verdet Constants are Determined by the Slopes of Each Line.

5.4 Imaging of Transparent Objects

This section discusses the application of the Faraday Effect to the imaging of transparent objects. The problem of stress in sample cuvettes is first described, and then the results of imaging three transparent fluids is presented.

5.4.1 Stress in Materials

The use of stress to modulate the optical properties of a material was briefly discussed in Chapter 2. Although it was not chosen as a modulation technique, its effect must be considered in the Faraday Effect imager. Figure 5-4 is a false color image constructed from the absolute light intensity (no modulation) transmitted through an empty plastic cuvette in the Faraday Effect imager. The rainbow pattern arises from the stress induced in the plastic rotating the plane of polarization. As demonstrated here, this effect would undermine measurements of the Faraday Effect. The use of annealed glass cuvettes solves this problem, as demonstrated in the next section.

5.4.2 Resolution of Transparent Objects

The scanning system was used to image a variety of liquid samples; this subsection demonstrates the imaging of three transparent fluids. The materials of interest were placed in standard 10mm glass cuvettes (annealed) and then scanned through the beam path. In Figure 5-5, a false color image illustrates the lack of significant amplitude modulation between the three transparent liquids; from left to right the fluids are carbon disulfide, water, and o-Xylenes. Any significant variations are indistinguishable from the instrument's noise.

Upon application of a 100 gauss magnetic field modulated at 12Hz, the differences between the three samples are easily observed through polarization rotation, as illustrated in Figure 5-6. Although the resolution of the experiment is only 1mm currently, these images do demonstrate the benefits of using the modulated Faraday Effect for the imaging of transparent materials.

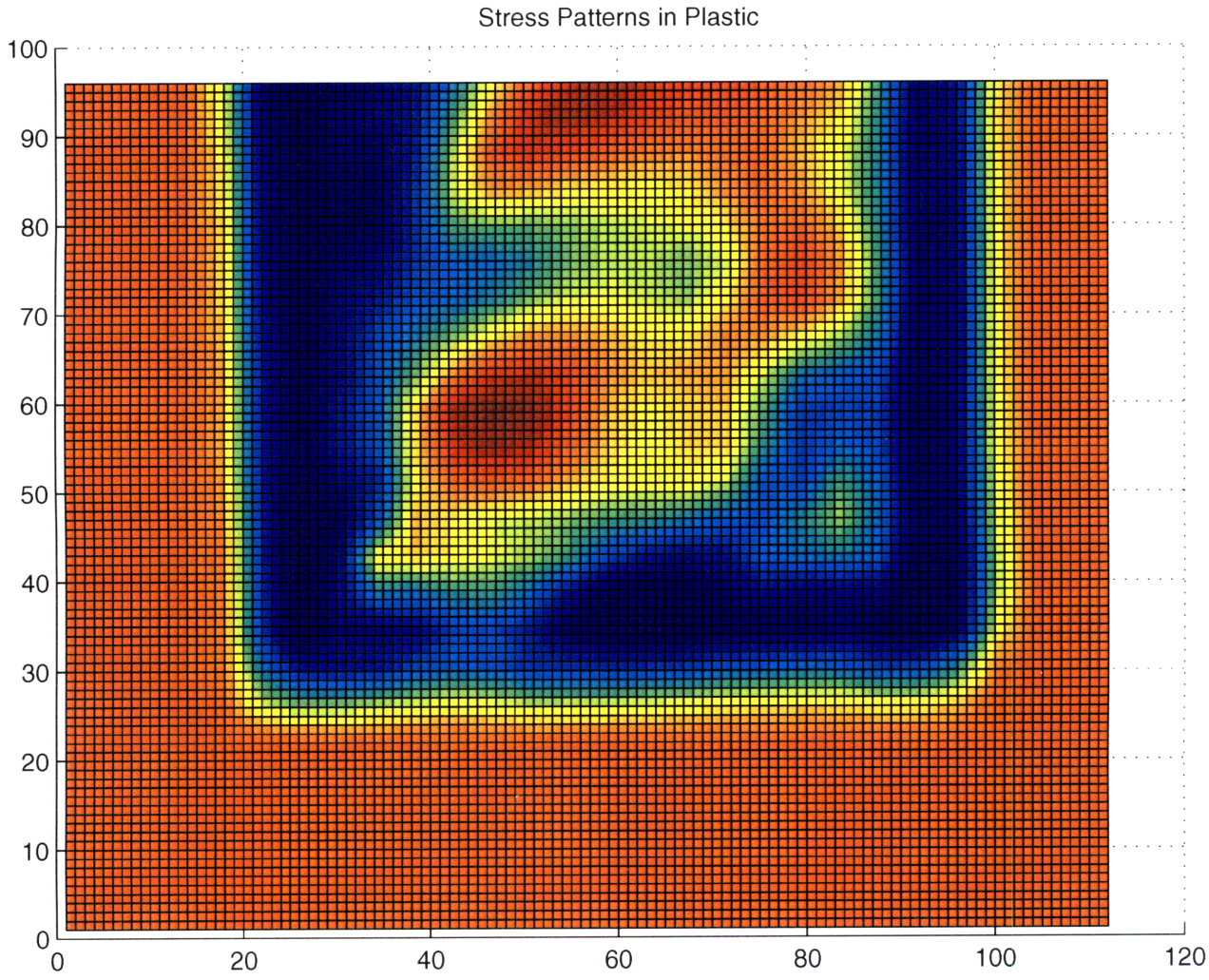

Figure 5-4: Imaging of the Stress Pattern in a Plastic Cuvette. The Image Represents the Absolute Light Intensity Transmitted through the Imager.

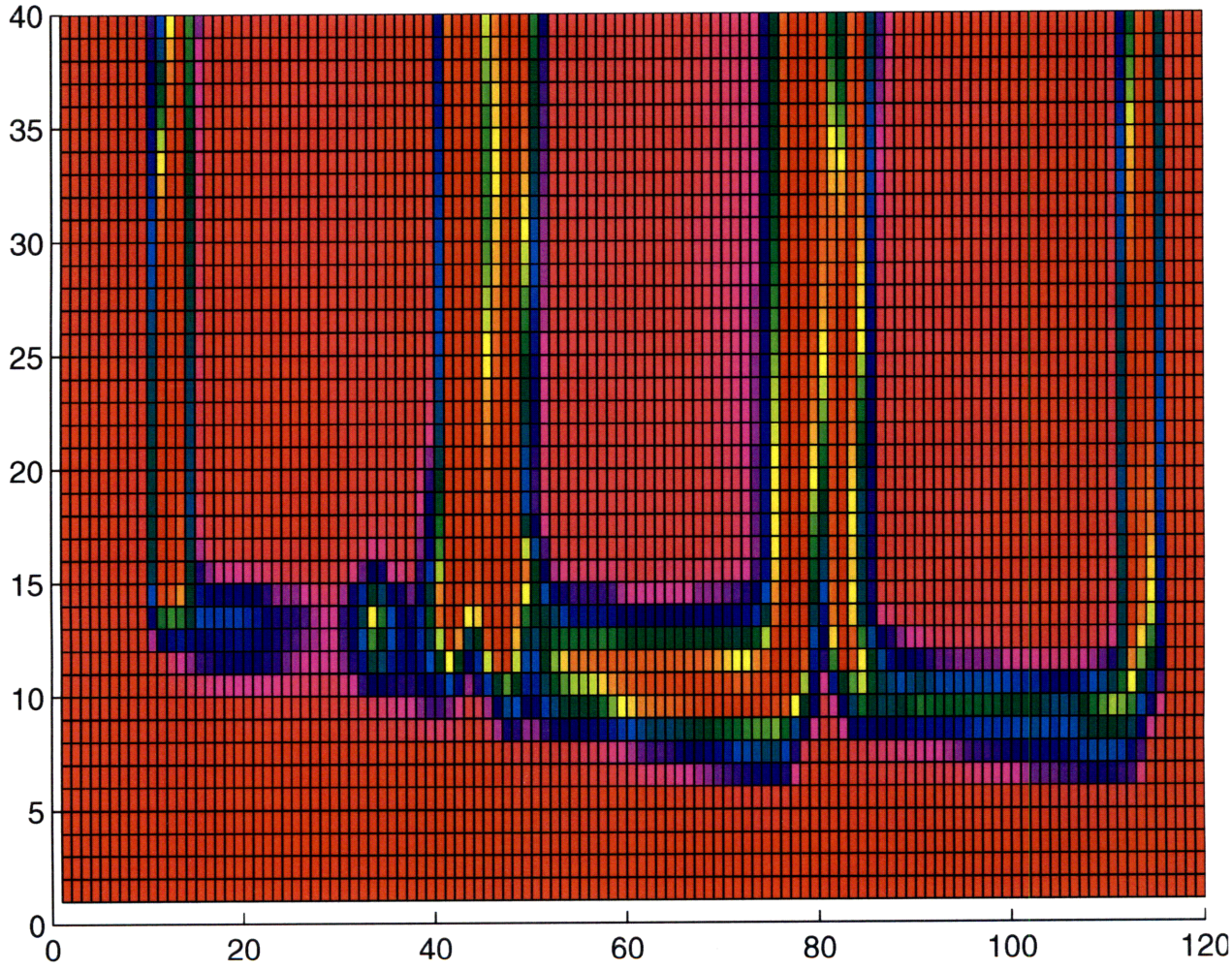

Figure 5-5: Image formed from amplitude measurements of two liquid samples. Small variations in materials are embedded in noise.

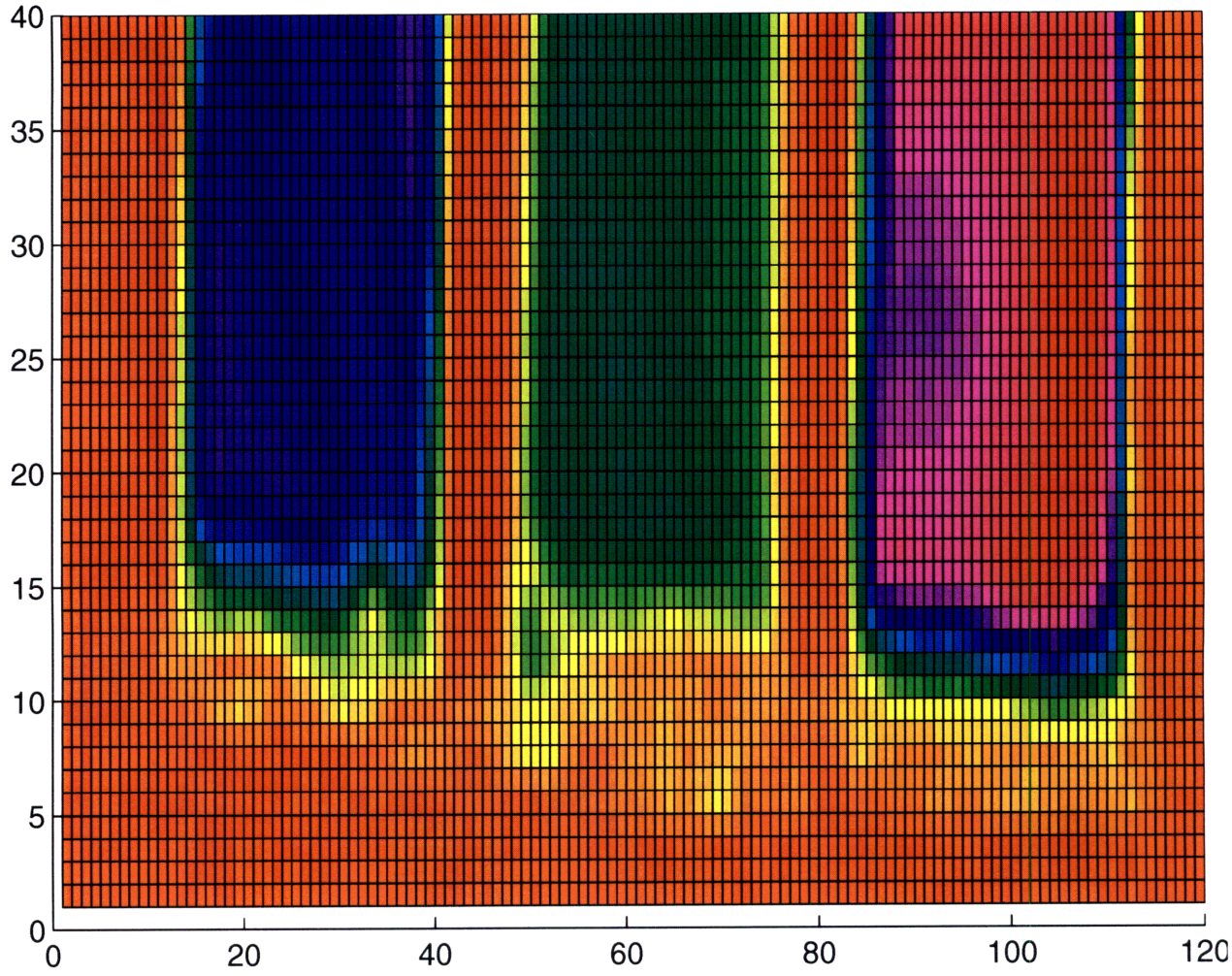

Figure 5-6: Image formed from use of synchronously-detected Faraday rotation in the samples. Small differences between the samples are now clearly observable.

5.5 Future Directions

Given the initial success of the Faraday effect contrast technique, it is currently being adapted to pursue the following research areas.

- Explore the effect of different optical wavelengths. In addition to studying the general spectral structure of samples, wavelengths that exhibit the highest degree of polarization rotation in media of interest, e.g., biological tissue, chemical samples, may be discovered.
- Decrease the scan time for two-dimensional sample scans.
- Develop tomographic techniques using, for example, long-wavelength (infra-red) light for deep penetration of biological tissues that will permit three dimensional imaging of samples.
- Using improved instrumentation, determine the effects of chemical and biological changes of interest on observed two and three dimensional Faraday scans. For example, it might be possible to determine the level of glucose saturation in the blood stream using deep penetration Faraday scans.
- Study and exploit the relationship between the induced Faraday rotation effect and the natural optical activity in common organic compounds.

Chapter 6

Summary

This thesis successfully demonstrated the use of the Faraday effect as a contrast mechanism for transparent materials. The use of external modulation of a material's optical properties allow them to be shifted outside of the region of large 1/F noise. Synchronous detection of this optical signal then allows for increased resolution of small optical variations in materials. Several methods of modulation were discussed, including stress, electric and magnetic fields. Of these, it was found that the Faraday effect was the most practical to implement.

The advantages of the Faraday effect for external modulation include the rapid penetration of an external magnetic field into a sample and the large range of Verdet constants. These principles were employed in a polarization sensitive instrument that externally modulated a magnetic field. The transmitted light intensity was then synchronously detected with respect to the varying field. This instrument established contrast in transparent materials that could not be differentiated by their amplitude modulation properties. Future applications of this contrast approach include the imaging of translucent tissues and structures at deeply penetrating wavelengths.

Appendix A

Circuit Schematics

A.1 Stepper Motor Interface Board

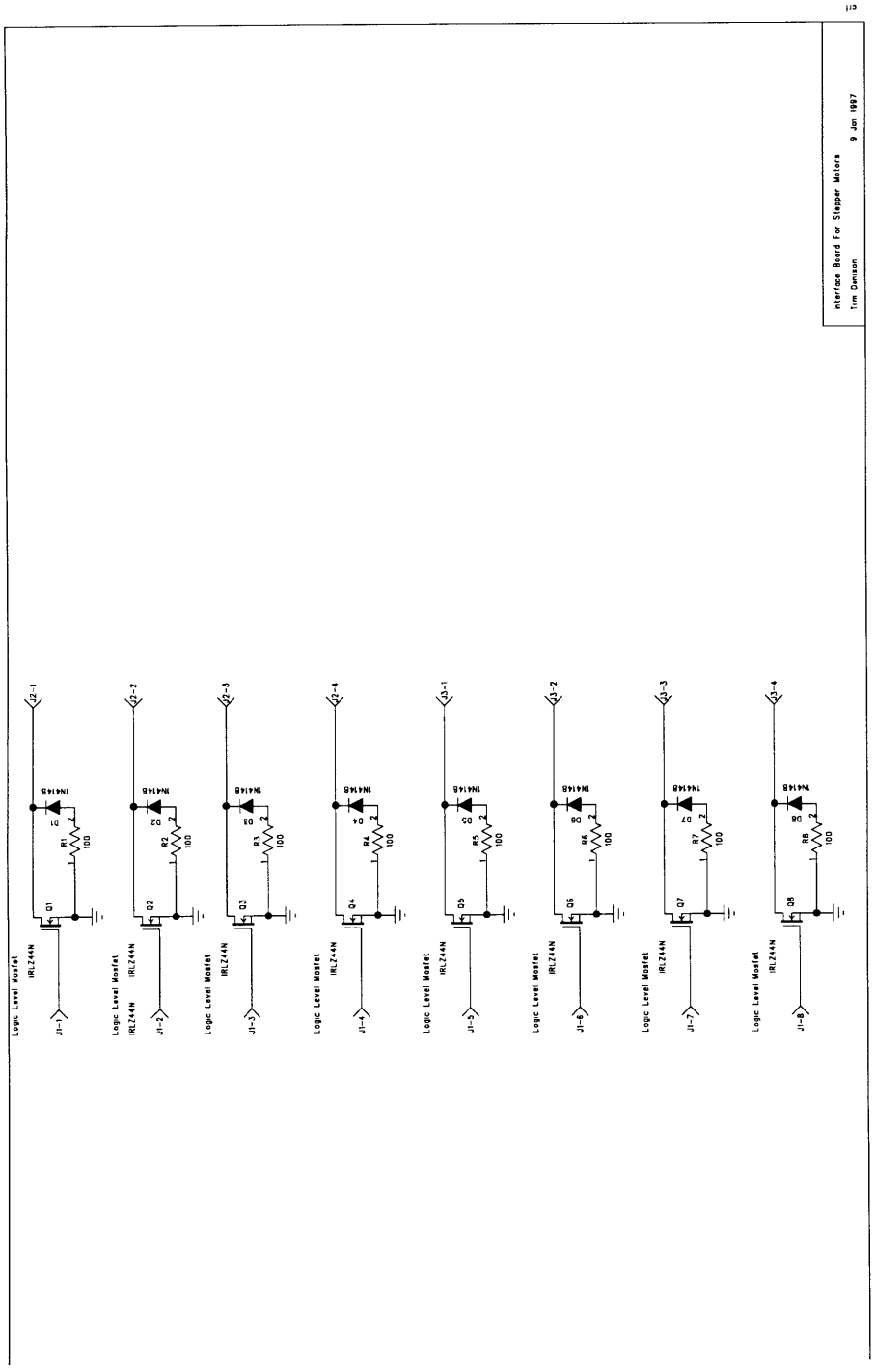

A.2 Full-Bridge with Driver

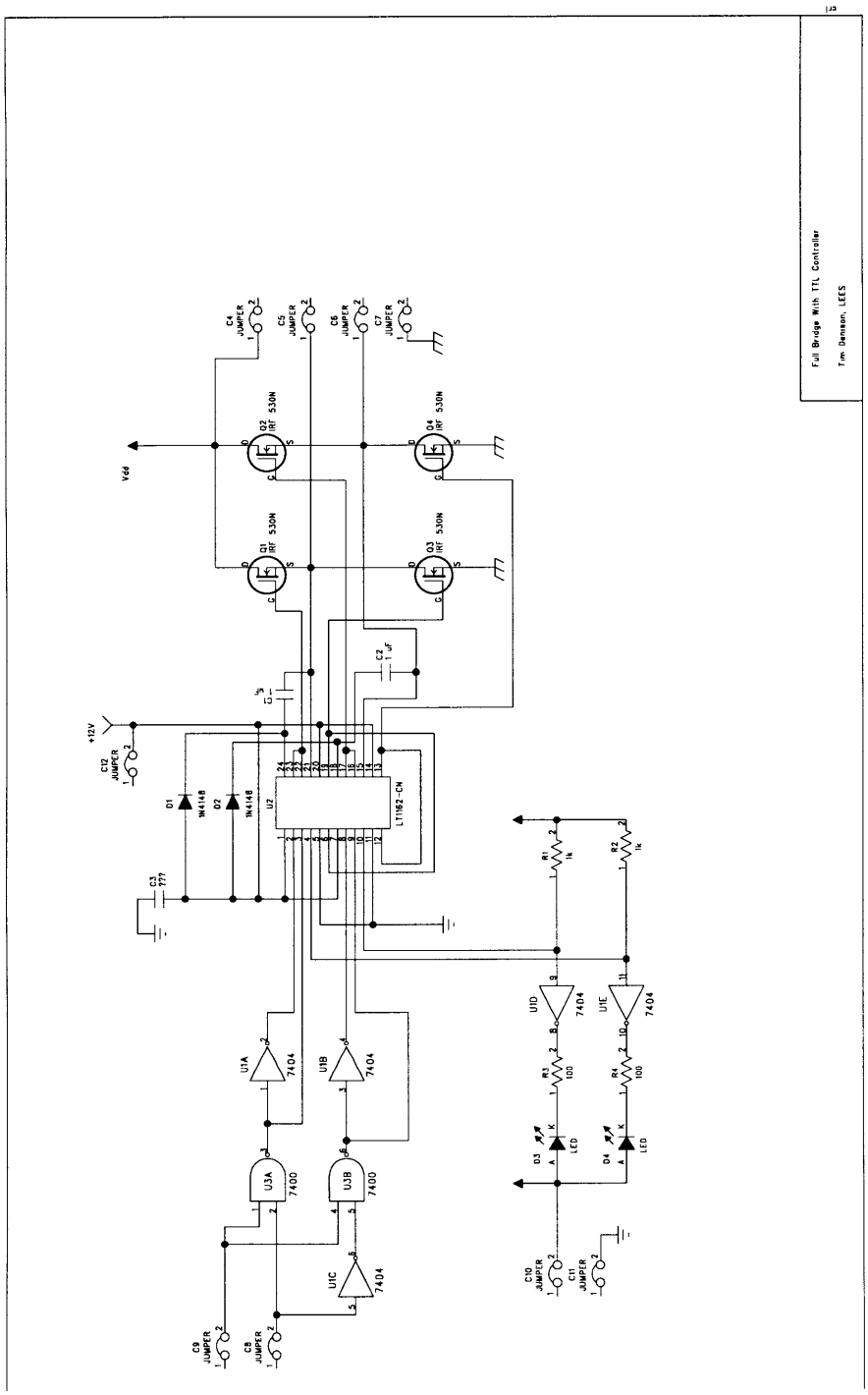

A.3 Notched Synchronous Detector

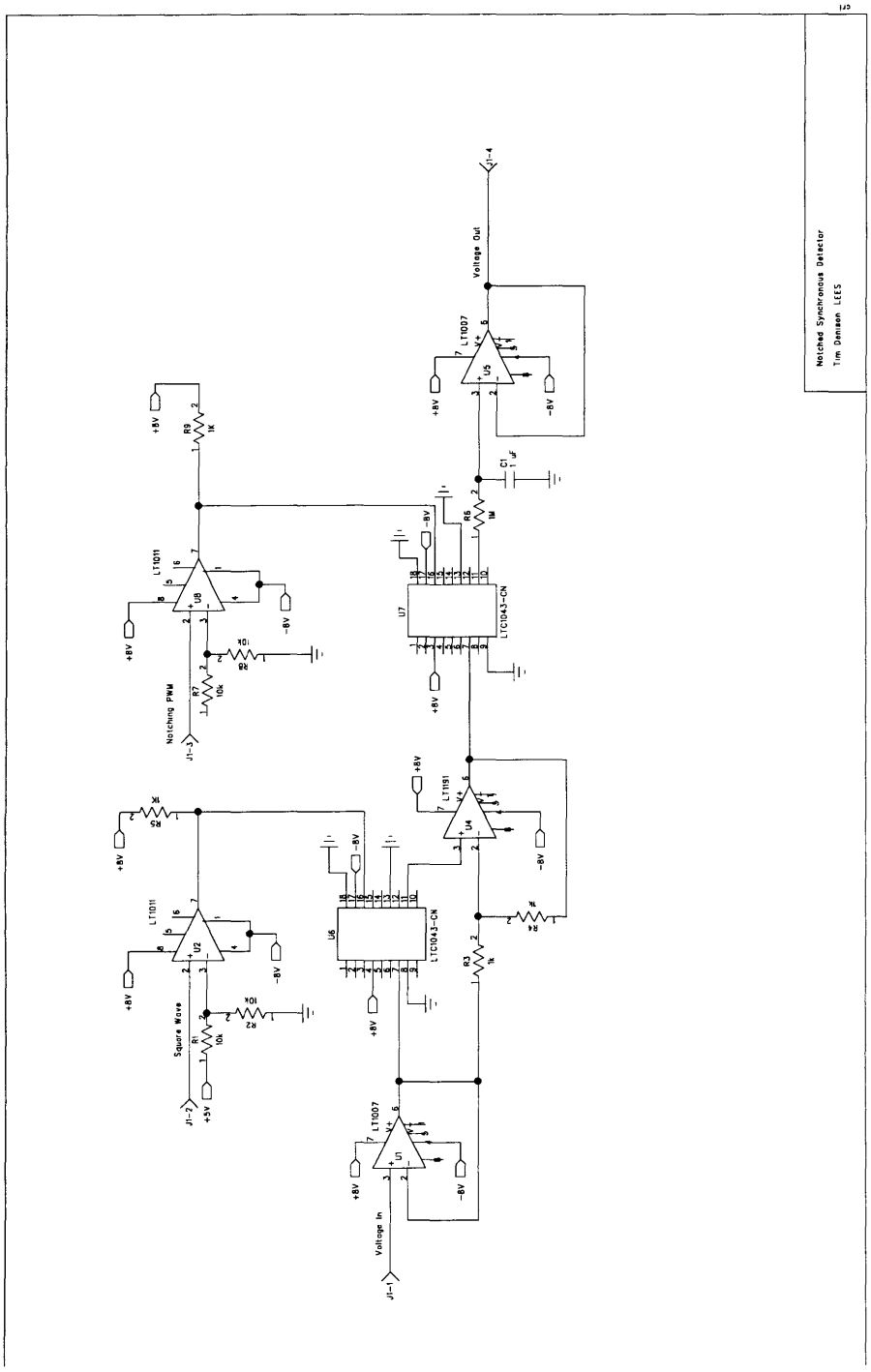

Appendix B

Software Codes

B.1 Data Acquisition Board

B.1.1 ADCCONFIG.C: Configure A/D Board

This program links with MATLAB to create a command "adcconfig." This sets the channel scanning, A/D range control, trigger source, and enables the pacer from the Genie's 8254 to trigger the A/D conversion.

```
/*Program to Configure the Genie Card through MATLAB MEX File*/
/*Interfaces to Tim's Synchronous Detector: Range (+/- 5V) */
/*Sampling Frequency provided by 8254 on Genie Card*/
/*Tim Denison  1997*/

#include <stdio.h>
#include "mex.h"

/*Globals for Addressing the Genie Card*/
unsigned int BASE = 0x300;
unsigned int LOW = 0x000;
unsigned int HIGH = 0x001;
unsigned int MUX = 0x002;
```

```
unsigned int INT = 0x008;
unsigned int CONTROL = 0x009;
unsigned int PACER = 0x010;

/*Interface of Program and MATLAB*/
void mexFunction(int nlhs, mxArray *plhs[], int nrhs, const mxArray *prhs[])
        {
configureBoard();
        printf("\nBoard configured\n");
        }

/*This Function Configures the Genie Board*/

void configureBoard(void)
        {
        /*Set the MUX address for Gain Control*/
        outp(BASE+MUX,0x00);

        /*Adjust the A/D Range Control*/
        outp(BASE+HIGH,0x00);

        /*Make the Board hardware triggered; sampling rate from cntconfig.c*/
        outp(BASE+CONTROL, 0x03);

        /*Enable the PACER for sampling trigger of ADC*/
        outp(BASE+PACER,0x00);
         }
```

B.1.2 CNTCONFIG.C: Configure 8254 Clock

This program links with MATLAB to create a command "cntconfig(xx)", where "xx" is a number that divides the 100kHz base clock. For example, cntconfig(100) results in a 1kHz clock that will pace the A/D convertor.

```
/*Program to Configure the Genie Card through MATLAB MEX File*/
/*8254 Counter used with 1MHz Base Clock to Derive ADC sampling trigger*/
/*Tim Denison  1997*/
/*To configure BOARD*/
#include <stdio.h>
#include "mex.h"

/*Globals for Addressing the Genie Card*/
unsigned int BASE = 0x300;
unsigned int LOW = 0x000;
unsigned int HIGH = 0x001;
unsigned int MUX = 0x002;
unsigned int INT = 0x008;
unsigned int CONTROL = 0x009;
unsigned int COUNT0 = 0x00C;
unsigned int COUNT1= 0x00D;
unsigned int COUNT2= 0x00E;
unsigned int COUNTC= 0x00F;
unsigned int PACER = 0x00A;


/*Interface of Program and MATLAB*/
void mexFunction(int nlhs, mxArray *plhs[], int nrhs, const mxArray *prhs[])
        {
```

```
        char *range,*trigger;
        int *channel, *start, *stop;
        double *data;

/*Get Pointer to Config Data*/
        data=mxGetPr(prhs[0]);

        /*Send Control Words to the Counter on 8254*/
        /*Standard 8254 Stuff*/

        /*Enable PACER*/
        outp(BASE+PACER, 0x00);

        /*Counter 1, Read/Write LSB first, then MSB; Rate Generator MODE*/
        /*Binary Mode Counting*/
        outp(BASE+COUNTC, 0x76);

        /*Send Out the Count, 100, which gives base clock of*/
        /*100.0kHz; to adjust, change counter 2 via MATLAB*/

        /*Output Low Byte*/
        outp(BASE+COUNT1, 0x0A);
        /*Output High Byte*/
        outp(BASE+COUNT1, 0x00);

        /*Send out Control Word to Counter2; same as COUNTER1,*/
        /*but the actual count value from MATLAB; final freq=10k/(*data)*/
        outp(BASE+COUNTC, 0xB6);

        /*Output Low Byte*/
```

```
 outp(BASE+COUNT2, (int)(*data));
 /*Output High Byte*/
 outp(BASE+COUNT2, 0x00);
}
```

B.1.3 FETCH2.C: Fetch Data from Board

This program links with MATLAB to create a function "fetch2(n)", where "n" is the number of samples. The current implementation is a 1Xn array.

```
/*Program to Fetch Data from the Genie Card through MATLAB MEX File*/
/*Data Returned in 1Xn vector; n samples determined by the user*/
/*Compiled as MEX with WATCOM C/C++*/
/*Tim Denison  1997*/
/*Note: Boards configured earlier with call to "goconfig.mex"*/

#include <stdio.h>
#include "mex.h"

/*Globals for Addressing the Genie Card*/
unsigned int BASE = 0x300;
unsigned int LOW = 0x000;
unsigned int HIGH = 0x001;
unsigned int MUX = 0x002;
unsigned int INT = 0x008;
unsigned int CONTROL = 0x009;


/*Interface of Program and MATLAB*/
void mexFunction(int nlhs, mxArray *plhs[], int nrhs, const mxArray *prhs[])
        {
```

```
double *volts, *voltage1;
int highbyte, lowbyte, i;
unsigned int m=1, n=2;
double *data;

        /*Get Pointer to Config Data*/
        data=mxGetPr(prhs[0]);

        /*Assign Size of Sample*/
        n = *data;

        /*Get Pointer to Matrix to Send Data to MATLAB*/
        plhs[0]= mxCreateDoubleMatrix(m,n,mxREAL);
        /*Set Pointer to MATLAB vector*/
        volts = mxGetPr(plhs[0]);

        /*Collect Samples*/
        for (i=0; i<n; i++) {

        /*Conversion now initiated from 8254 (7/26/97)*/
        /*outp(BASE,0);*/

        /*Wait For Interupts to Signal Conversion*/
        /*Mask with bit5, Interupt Vector*/
        while(!(inp(BASE+INT) & 0x10));

        /*Get the Data*/
        highbyte=inp(BASE+HIGH);
        lowbyte=inp(BASE+LOW);
```

```
                /*Reset the ADC Board*/
                outp(BASE+INT, 0);

                /*Do Bit-> Voltage Conversion*/
                goConvert(highbyte, lowbyte, volts);

                /*Increment pointer for MATLAB vector*/
                volts++;

                }
        }

/*This Function Converts the Two-byte Data into a */
/* Voltage and Channel Number*/

void goConvert(int highbyte, int lowbyte, double *volts) {
        long int totalbyte;
        /*This is determined by the Genie Protocol*/
/*See manual for details*/
        /*Shift high byte up by 4*/
        highbyte = highbyte << 4;

/*Mask out channel info in low byte, shift down by 4*/
        lowbyte = lowbyte & 0xF0;
        lowbyte = lowbyte >> 4;
        totalbyte = highbyte + lowbyte;
        *volts = ((10 * (double)totalbyte/4096) + (-5));
        }
```

B.2 GOLEFT.C: Steeper Motor Interface Code

```
/*Program to Configure the Genie Card through MATLAB MEX File*/
/*Drives Stepper Motors through the Stepper Interface Board*/
/*Tim Denison  1997*/
#include <stdio.h>
#include "mex.h"

/*Globals for Addressing the Genie Card*/
unsigned int BASE = 0x300;
unsigned int LOW = 0x000;
unsigned int HIGH = 0x001;
unsigned int MUX = 0x002;
unsigned int INT = 0x008;
unsigned int CONTROL = 0x009;
unsigned int DIGITAL1 = 0x003;
unsigned int DIGITAL2 = 0x00B;

/*Interface of Program and MATLAB*/
void mexFunction(int nlhs, mxArray *plhs[], int nrhs, const mxArray *prhs[])
        {
        unsigned int m=1, n=2, i, k;
        double *data, *volts;

        /*Set Pointer to Input Matrix from MATLAB*/
        data=mxGetPr(prhs[0]);

/*Rotate number of cycles pointed to by data*/
        for(i=0; i < *data; i++) {
        /*Rotate Through Cycle*/
                outp(BASE+DIGITAL1, 0x30);
```

```
                /*delay*/
                for(k=0; k<500000; k++);

                outp(BASE+DIGITAL1, 0x60);
                for(k=0; k<500000; k++) ;

                outp(BASE+DIGITAL1, 0xC0);
                for(k=0; k<500000; k++);

                outp(BASE+DIGITAL1, 0x90);
                for(k=0; k<500000; k++);
        }
}
```

B.3 Sample Experiment: MATLAB Scan Code

A sample experiment that creates a two-dimensional image of a sample based on its Faraday Effect.

```
function data = scan(numpointsx, scanstepx,numpointsy,scanstepy,samples);
% data = scan2d(numpointsx, scanstepy,numpointsy,scanstepy,samples);
% SCAN2D is the master control program for the Faraday Scanning
% Imager System: Fills in Matrix of points while controlling scanner
% Uses .MEX files created for Genie Card
% to move scan stage and acquire, average data
% Tim Denison 8/97


for i=1:numpointsy
   for n=1:numpointsx
```

```
    goleft(scanstepx);
    buffer = fetch2(samples);
    data(i,n) =  mean(buffer);
    end;
goright(scanstepx.*(numpointsx));
goup(scanstepy);
end;
godown((numpointsy).*scanstepy);
```

Appendix C

Time Domain Examples of Notching

The following plots illustrate the use of a 210-bit magic sinewave to eliminate the sensitivity to odd-harmonics of the fundamental frequency. In each figure, the top trace is the demodulation waveform, the bottom trace is the sinusoid being demodulated, and the middle trace is the unfiltered output of the demodulator. The net DC content of the middle trace represents the sensitivity to that harmonic.

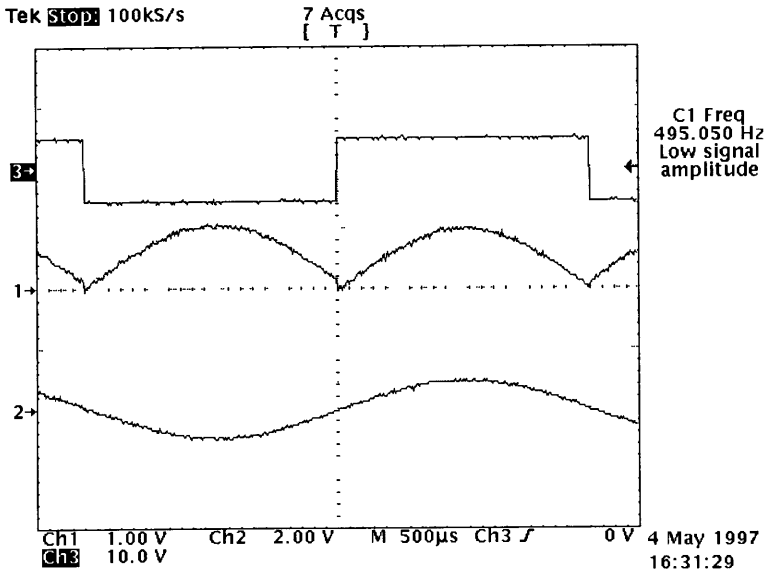

Figure C-1: Standard synchronous demodulation of the fundamental with a square wave.

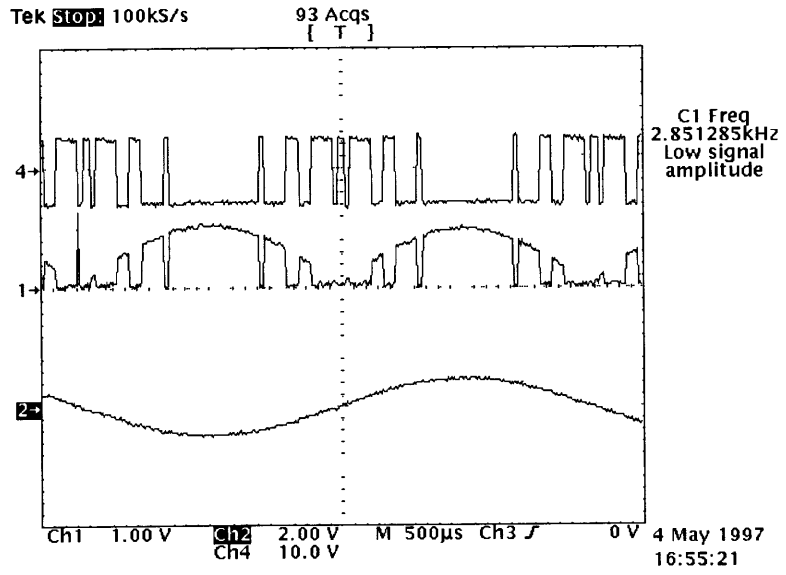

Figure C-2: Synchronous demodulation of the fundamental with 210-bit magic sinewave. DC component (sensitivity) is slightly reduced.

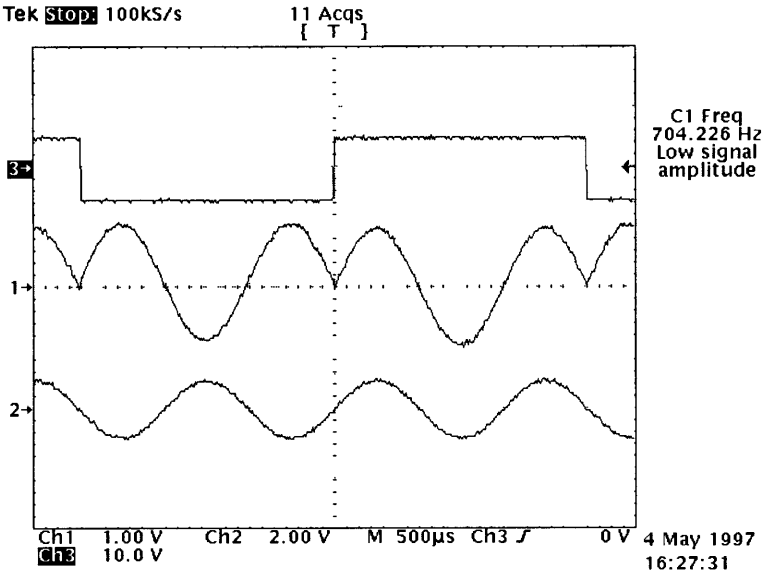

Figure C-3: Synchronous demodulation of the third harmonic with a square wave. Note substantial DC component in the output waveform.

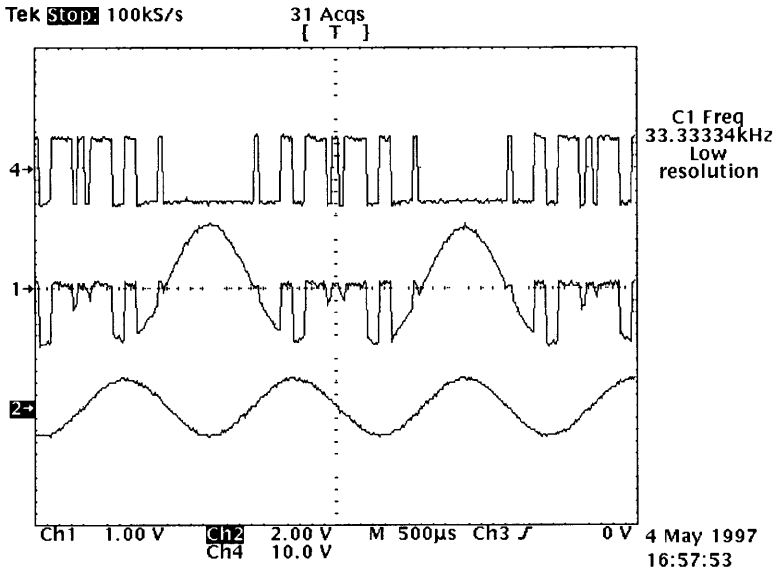

Figure C-4: Synchronous demodulation of third harmonic with 210-bit magic sinewave. Note dramatic reduction of DC component of the middle trace (sensitivity).

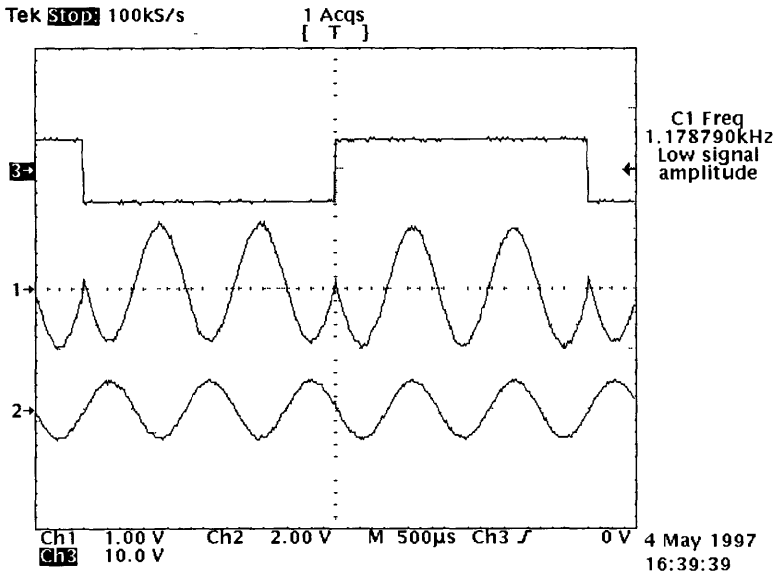

Figure C-5: Synchronous demodulation of the fifth harmonic with a square wave. Note substantial DC component in the output waveform.

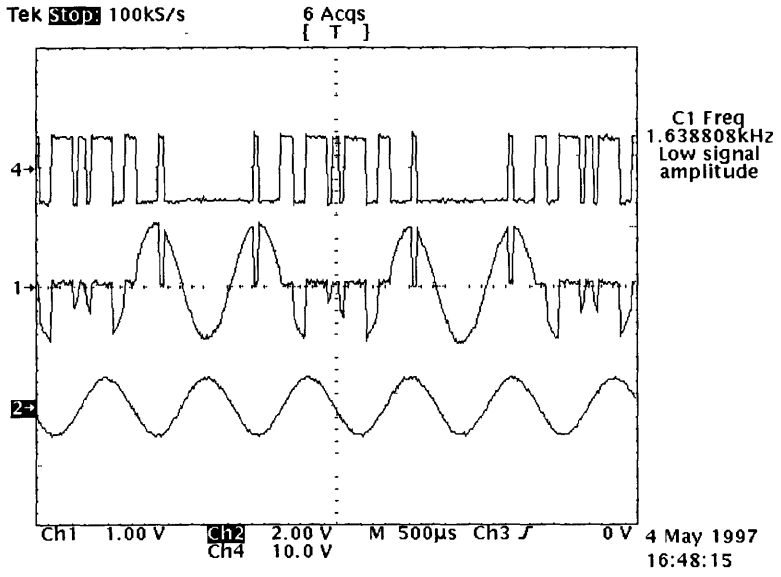

Figure C-6: Synchronous demodulation of the fifth harmonic with 210-bit magic sinewave. Note dramatic reduction of the DC component of the middle trace (sensitivity).

Bibliography

[1] G.W. Day and M. N. Deeter. Faraday effect sensors for magnetic field and electric current. *SPIE: Fiber Optic and Laser Sensors XII*, 2292:42–47, 1994.

[2] F. G. Dunnington. *Physical Review*, page 1506, 1931.

[3] W. Rave F. Schmidt and A. Hubert. Enhanecement if magneto-optical domain observtion by digital image processing. *IEEE Transactions on Magnetics*, 21(5):1596–1598, 1985.

[4] M. Faraday. Experimental researches in electricity; on the magnetization of light and the illumination of magnetic lines of force. *Philosophical Transactions of 1846-1852*, 1855.

[5] R. Feynman. *The Feynmann Lectures on Physics.* Addison-Wesley, 1965.

[6] C.A. Fowler and E.M. Fryer. Magnetic domains by the longitudinal kerr effect. *Physical Review*, 94(1):52–56, 1954.

[7] G. Fowles. *Introduction to Modern Optics.* Holt, Rinehart and Winston, 1975.

[8] R. Goldstein. Pockels cell primer. *Laser Focus Magazine*, 1968.

[9] P. R. Gray and R. Meyer. *Analysis and Design of Analog Integrated Circuits.* John Wiley and Sons, 1993.

[10] C. Enke H. Malmstadt and S. Crouch. *Electronics and Instrumentation for Scientists.* Benjamin/Cummings Publishing, 1981.

[11] E. Hecht. *Optics.* Addison-Wesley Publishing, 1987.

[12] A. Honda and K. Shirae. Domain pattern measurements using ccd. *IEEE Transactions on Magnetics*, 17(6):3096–3098, 1981.

[13] P. Horowitz and W. Hill. *The Art of Electronics.* Cambridge University Press, 1989.

[14] G. Verghese J. Kassakian, M. Schlecht. *Power Electronics.* Academic Press, 1991.

[15] J.D. Jackson. *Classical Electrodynamics.* John Wiley and Sons, 1975.

[16] F. Jenkins and H. White. *Fundamentals of Optics.* McGraww-Hill, 1976.

[17] D. Lancaster. Resource bin #54. *http://www.tijana.com.*

[18] F. J. Loeffler. Faraday rotation experiment for the undergraduate physics laboratory. *American Journal of Physics*, 51(7):661–663, 1983.

[19] H. A. Lorentz. *The theory of electrons and its applications to the phenomenaof light and radiant heat.* Dover Publications, 1952.

[20] MIT Dept. of Physics. Junior lab project: Faraday rotation.

[21] B. Petek P.L. Trouilloud and B.E. Argyle. Methods for wide-field kerr imaging of small magnetic domains. *IEEE Transactions on Magnetics*, 30(6):4494–4496, 1994.

[22] Prins and Van der Wielen. Magneto-optical faraday effect probed in a scanning tunneling microscope. *IEEE Transactions on Magnetics*, 30(6):4491–4493, 1994.

[23] J. Roberge. Personal communication.

[24] K. Ross. *Phase contrast and interference microscopy for cell biologist.* St. Martin's Press, 1967.

[25] S. Shaw. Personal communication.

[26] A. Sommerfeld. *Optics: Lectures on Theoretical Physics, Vol. IV.* Academic Press, 1954.

[27] K.-H. Feller V. Bruckner and U.-W. Grummt. *Applications of Time-Resolved Optical Spectroscopy.* Elsevier, 1990.

[28] E. Hill W. Clegg, N. Heyes and C. Wright. Development of a scanning laser microscope for magneto-optic studies of thin magnetic films. *Journal of Magnetism and Magnetic Materials*, 95:49–57, 1991.

[29] S. H. Zaidi and R. P. Tatam. Farady-effect magnetometry: compensation for the temperature-dependent verdet constant. *Measurement Science and Technology*, 5:1471–1479, 1994.

[30] F. Zernicke. *Physica I*, page 689, 1934.